UPPSALA
UNIVERSITET

*Digital Comprehensive Summaries of Uppsala Dissertations from the Faculty of Science and Technology* 1701

# The Multiple Faces of Interfaces

## *Electron microscopy analysis of $CuInSe_2$ thin-film solar cells*

OLIVIER DONZEL-GARGAND



ACTA
UNIVERSITATIS
UPSALIENSIS
UPPSALA
2018

ISSN 1651-6214
ISBN 978-91-513-0402-1
urn:nbn:se:uu:diva-357127

Dissertation presented at Uppsala University to be publicly examined in Polhemssalen, The Angstromlaboratory, Lägerhyddsvägen 1, Uppsala, Friday, 28 September 2018 at 09:30 for the degree of Doctor of Philosophy. The examination will be conducted in English. Faculty examiner: Dr. Daniel Abou-Ras (Helmholtz-ZentrumBerlin (HZB) Department Nanoscale structures and microscopic analysis ).

**Abstract**
Donzel-Gargand, O. 2018. The Multiple Faces of Interfaces. Electron microscopy analysis of $CuInSe_2$ thin-film solar cells. *Digital Comprehensive Summaries of Uppsala Dissertations from the Faculty of Science and Technology* 1701. 85 pp. Uppsala: Acta Universitatis Upsaliensis. ISBN 978-91-513-0402-1.

The CIS solar cell family features both a high stability and world-class performances. They can be deposited on a wide variety of substrates and absorb the entire solar spectrum only using a thickness of a few micrometers. These particularities allow them to feature the most positive Energy returned on energy invested (EROI) values and the shortest Energy payback times (EPBT) of all the main photovoltaic solar cells. Using mainly electron microscopy characterization techniques, this thesis has explored the questions related to the interface control in thin-film photovoltaic solar cells based on $CuInSe_2$ (CIS) absorber materials. Indeed, a better understanding of the interfaces is essential to further improve the solar cell conversion efficiency (currently around 23%), but also to introduce alternative substrates, to implement various alloying (Ga-CIS (CIGS), Ag-CIGS (ACIGS)…) or even to assess alternative buffer layers.

The thread of this work is the understanding and the improvement of the interface control. To do so, the passivation potential of $Al_2O_3$ interlayers has been studied in one part of the thesis. While positive changes were generally measured, a subsequent analysis has revealed that a detrimental interaction could occur between the NaF precursor layer and the rear $Al_2O_3$ passivation layer. Still within the passivation research field, incorporation of various alkali-metals to the CIS absorber layer has been developed and analyzed. Large beneficial effects were ordinarily reported. However, similar KF-post deposition treatments were shown to be potentially detrimental for the silver-alloyed CIGS absorber layer. Finally, part of this work dealt with the limitations of the thin-barrier layers usually employed when using steel substrates instead of soda-lime glass ones. The defects and their origin could have been related to the steel manufacturing process, which offered solutions to erase them.

Electron microscopy, especially Transmission electron microscopy (TEM), was essential to scrutinize the local changes occurring at the different interfaces within a few nanometers. The composition variation was measured with both Electron energy loss spectroscopy (EELS) and Energy dispersive X-ray spectroscopy (EDS) techniques. Finally, efforts have been invested in controlling and improving the FIB sample preparation, which was required for the TEM observations in our case.

*Keywords:* Electron microscopy, TEM, STEM, EELS, EDS, solar cells, CIGS, ACIGS, CZTS, post deposition treatment, KF, RbF, buffer layers, interfaces, inter layers, barrier layers, passivation layers

*Olivier Donzel-Gargand, Department of Engineering Sciences, Applied Materials Sciences, Box 534, Uppsala University, SE-75121 Uppsala, Sweden. Department of Engineering Sciences, Solid State Electronics, Box 534, Uppsala University, SE-75121 Uppsala, Sweden.*



ISSN 1651-6214
ISBN 978-91-513-0402-1
urn:nbn:se:uu:diva-357127 (http://urn.kb.se/resolve?urn=urn:nbn:se:uu:diva-357127)

*Le vent se lève !... il faut tenter de vivre !*
*Paul Valéry*

to my friends, to my family

# List of Papers

This thesis is based on the following papers, which are referred to in the text by their Roman numerals.

Reprints were made with permission from the respective publishers.

I Joel, J., Vermang, B., Larsen, J., Donzel-Gargand, O., & Edoff, M. (2015). On the assessment of CIGS surface passivation by photoluminescence. *Physica Status Solidi - Rapid Research Letters*, *9*(5), 288–292. http://doi.org/10.1002/pssr.201510081

II Donzel-Gargand, O., Thersleff, T., Fourdrinier, L., Leifer, K., & Edoff, M. (2016). Surface defect passivation by a thin metallic barrier for Cu(InxGa1-x)Se2co-evaporation on Cr-steel substrates. *Thin Solid Films*, *619*, 220–226. http://doi.org/10.1016/j.tsf.2016.10.063

III Vermang, B., Ren, Y., Donzel-Gargand, O., Frisk, C., Joel, J., Salome, P., … Edoff, M. (2016). Rear surface optimization of CZTS solar cells by use of a passivation layer with nanosized point openings. *IEEE Journal of Photovoltaics*, *6*(1), 332–336. http://doi.org/10.1109/JPHOTOV.2015.2496864

IV Donzel-Gargand O, Thersleff T, Keller J, et al. Deep surface Cu depletion induced by K in high-efficiency Cu(In,Ga)Se2 solar cell absorbers. *Prog. Photovoltaics Res. Appl.* 2018. doi:10.1002/pip.3010.

V Donzel-Gargand O, Larsson F, Törndahl T, Stolt L, Edoff M. (Submitted) Surface Modification And Secondary Phase Formation From a High Dose KF-Post Deposition Treatment of (Ag,Cu)(In,Ga)Se2 Solar Cell Absorbers.

VI Ledinek D, Donzel-Gargand O, Sköld M, Keller J, Edoff M. Effect of different Na supply methods on thin Cu(In,Ga)$Se_2$ solar cells with Al2O3 rear passivation layers. *Sol. Energy Mater. Sol. Cells* 2018;187(May):160-169. doi:10.1016/j.solmat.2018.07.017

# Other contributions

I Ajalloueian, F., Tavanai, H., Hilborn, J., Donzel-Gargand, O., Leifer, K., Wickham, A., & Arpanaei, A. (2014). Emulsion electrospinning as an approach to fabricate PLGA/chitosan nanofibers for biomedical applications. *BioMed Research International*, *2014*, 475280. http://doi.org/10.1155/2014/475280

II Lindahl, J., Keller, J., Donzel-Gargand, O., Szaniawski, P., Edoff, M., & Törndahl, T. (2016). Deposition temperature induced conduction band changes in zinc tin oxide buffer layers for Cu(In,Ga)Se2solar cells. *Solar Energy Materials and Solar Cells*, *144*, 684–690. http://doi.org/10.1016/j.solmat.2015.09.048

III Englund, S., Paneta, V., Primetzhofer, D., Ren, Y., Donzel-Gargand, O., Larsen, J. K., … Platzer Björkman, C. (2017). Characterization of TiN back contact interlayers with varied thickness for Cu2ZnSn(S,Se)4 thin film solar cells. *Thin Solid Films*, *639*, 91–97. http://doi.org/10.1016/j.tsf.2017.08.030

IV Bilousov, O. V., Ren, Y., Törndahl, T., Donzel-Gargand, O., Ericson, T., Platzer-Björkman, C., … Hägglund, C. (2017). Atomic Layer Deposition of Cubic and Orthorhombic Phase Tin Monosulfide. *Chemistry of Materials*, *29*(7), 2969–2978. http://doi.org/10.1021/acs.chemmater.6b05323

V Ren, Y. Y., Richter, M., Keller, J., Redinger, A., Unold, T., Donzel-Gargand, O., … Platzer Björkman, C. (2017). Investigation of the {SnS}/Cu2ZnSnS4 Interfaces in Kesterite Thin-Film Solar Cells. *{ACS} Energy Letters*, *2*(5), 976–981. http://doi.org/10.1021/acsenergylett.7b00151

VI Larsson F, Donzel-Gargand O, Keller J, Edoff M, Törndahl T. Atomic layer deposition of Zn(O,S) buffer layers for Cu(In,Ga)Se 2 solar cells with KF post-deposition treatment. Sol. Energy Mater. Sol. Cells 2018;183(3):8-15. doi:10.1016/j.solmat.2018.03.045.

VII Englund et al. (Submitted) TiN Interlayers with varied thickness in CZTS(e) Solar Cells: Effect on Na diffusion, back contact stability and Performance.

# Contents

# Abbreviations and Symbols

| | |
|---|---|
| ADF | Annular dark field |
| ALD | Atomic layer deposition |
| BF | Bright field |
| CBD | Chemical bath deposition |
| CBO | Conduction band offset |
| CIGS | $Cu(In,Ga)Se_2$ |
| ACIGS | $(Ag,Cu)(In,Ga)Se_2$ |
| CZTS | $Cu(Zn,Sn)S_2$ |
| DF | Dark field |
| DP | Diffraction pattern |
| EBIC | Electron beam induced current |
| EDS | Energy dispersive X-ray spectroscopy |
| EELS | Electron energy loss spectroscopy |
| EPBT | Energy payback time |
| EROI | Energy returned on energy invested |
| FIB | Focused ion beam |
| GDOES | Glow-discharge optical emission spectroscopy |
| GFIS | Gas field ion source |
| HAADF | High angle annular dark field |
| HLS | Heat light soaking |
| LMIS | Liquid metal ion source |
| OECD | Organization for Economic Co-operation and Development |
| PDT | Post-deposition treatment |
| PV | Photovoltaic |
| S-Q | Shockley-Queisser |
| SBR | Signal-to-Background Ratio |
| SEM | Scanning electron microscopy |
| SLG | Soda lime glass |
| SNR | Signal-to-Noise Ratio |
| STEM | Scanning TEM |
| TCO | Transparent conductive oxide |
| TEM | Transmission electron microscopy |
| XPS | X-ray photoelectron spectroscopy |

| | |
|---|---|
| XRD | X-ray diffraction |
| XRF | X-ray fluorescence |
| ZA | Zone Axis |
| ZLP | Zero Loss Peak |
| FF | Fill Factor |
| J | Current density |
| $J_{sc}$ | Short circuit current |
| $N_t$ | Trap density |
| $V_{oc}$ | Open circuit voltage |
| t | Lamella thickness |
| $\alpha$ | Convergence semi-angle |
| $\beta$ | Collection semi-angle |
| $\Delta$ | Energy range |
| $\chi$ | Electron affinity |
| $\phi$ | Work function |
| $\lambda$ | Wavelength |
| $\eta$ | Efficiency |
| $\sigma$ | Partial cross section |
| $t/\lambda$ | Relative thickness |

# 1 Introduction

## 1.1 Background

### 1.1.1 Energy conversion

"I'm a pessimist because of intelligence, but an optimist because of will" as written by Antonio Gramsci, is probably an excellent explanation of the scientific perseverance. The global picture is not pleasant to look at, as we will see in a minute, but we do it anyway trying to contribute to the existing solutions.

Receiving all the news about photovoltaic (PV) developments and electrical vehicles, I started to think that the world is now driven by renewables. However, the real picture is quite different. In 2016, about 85% of the energy consumed in the world is provided by fossil resources. Nuclear and hydropower represent about 11% and the remaining 4% is further divided between the diverse renewables (wind, solar, biofuel, biogas). Note that wood is excluded from this because it is not traded on the same markets. Solar energy represents then roughly 1% of the consumed energy in the world in 2016 as shown in Figure 1. But this energy consumption includes everything from solid to gaseous fuels. As our field is essentially competing in the electricity production part, I should try to be more specific. In the OECD countries, the electricity production is mainly relying on fossil fuels (60%), then comes nuclear power, hydroelectricity and finally the renewable sources [a] (8%). As a consequence our electric vehicles are mostly running on coal and gas, not as "green" as a human powered bicycle [1]. In 2017, the solar share of the world electricity production is about 2% [2]. While the actual importance of our solar energy is far from what I might have expected, one can find some comfort in the growth rate of the renewables over 14% in 2016, well above the global energy consumption growth 1.0% (2016) [3]. This highlights the actual progress achieved into the market share which is an excellent sign for photovoltaic applications.

[a] Renewables includes geothermal, solar, tide/wave/ocean and wind.

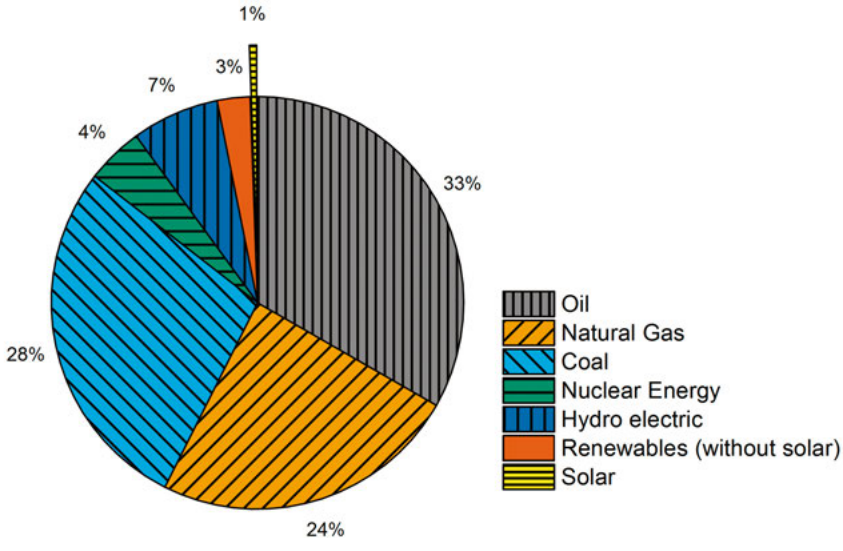


Figure 1 World energy consumption in 2016. The solar-based energy is represented by the exploded wedge. Data from British Petroleum (BP) statistical review of world energy (2017) [3]

As mentioned, the global energy consumption is still increasing but the fossil fuels will reach an end. There is a limited amount of resources buried underground and even a constant or "reasonable" consumption, whatever this means, will end it [b]. The simulations on the subject do not perfectly agree on the time remaining before the last liter of fuel would be burnt, but they show that the oil production peak is currently happening, and is already behind us for the conventional oil extraction. Concerning the coal, the production peak should happen in approximately one century. Subsequently, there are two vital projects to work on, to spare as much energy as we can, and to spend the remaining part on developing different and sustainable ways of converting the energy we need.

[b] c.f. the Hubbert peak theory

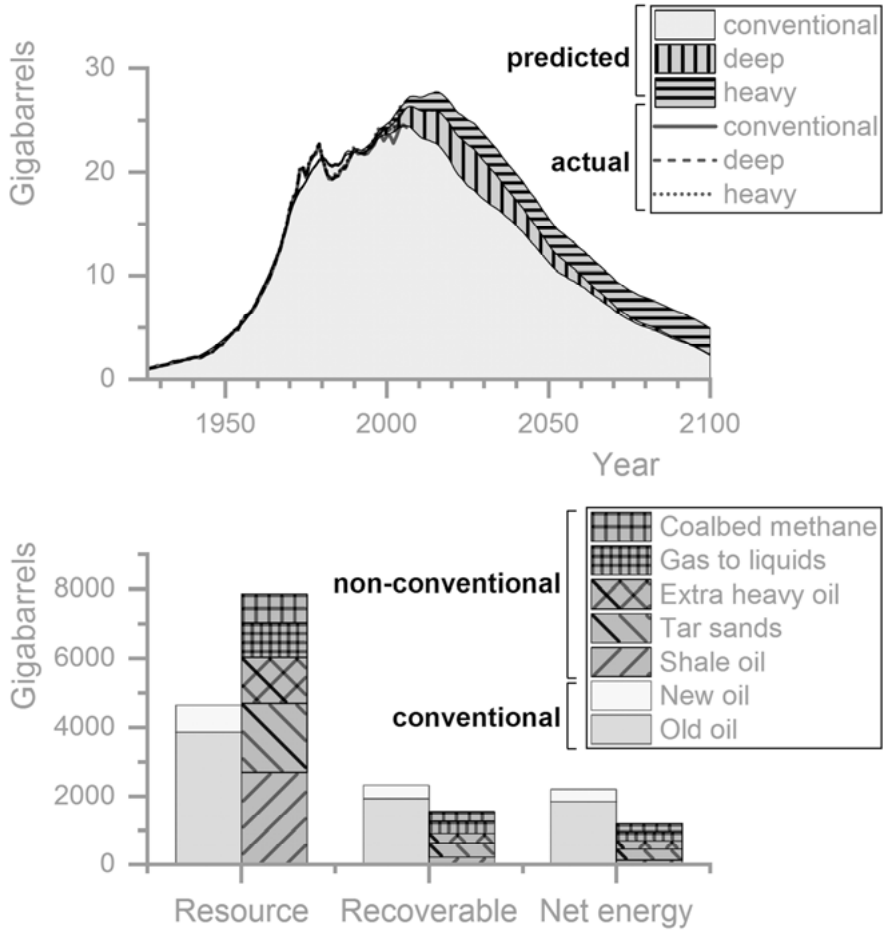


Figure 2 To the top, the world production of liquid fuels featuring the predicted and the actual production volumes. The production peak is expected to occur now. To the bottom, the graph shows the liquid fuel resources in each category, the recoverable part and the final accessible net energy. The net energy calculation accounts for the specific Energy return on Energy invested (EROI), for example at 23 and 2.5 for Old oil and Shale oil, respectively (source: *Transport Energy Futures: Long-Term Oil Supply Trends and Projections Report 117* (BITRE, 2009)) [4]

### 1.1.2 Role of Photovoltaic Solar Cells

PV energy conversion demonstrates serious assets such as the limited maintenance of an installation, the system scalability ranging from domestic use to industrial farm generators, the spread of energy production reinforcing the energy security, and the long lifespan of an installation (around 30 years). It is worth mentioning than unlike some energy conversion technologies, PV systems are all energetically interesting to produce as they show a

large Energy return of energy invested (EROI) and a low energy payback time (EPBT). This is especially true for the thin-film PV where the low manufacturing costs (energy-wise) are among the lowest and display EROI values from 15 to 30 times (!) and EPBT from 1.5 to 4 years [c]! [5,6] Added to the fact that solar irradiations come to us in huge quantities at no cost and we have an extremely potent combo.

The question related to price is indeed of interest but probably more political than scientific. If the price is a major problem nowadays, we ought to look more carefully at the rest of the picture because it may not be as predominant in a few decades.

PV energy conversion unfortunately also has drawbacks. The main one being that (with few exceptions) the sun sets every day, and, taking the view of the electric grid, does not seem to care about our need in electricity power supply. This fairly inflexible electricity conversion requires implementation of buffers both to absorb the energy converted that cannot be consumed and to provide electricity when the sun rests or plays hide-and-seek with the clouds. Of course there are ways to store energy but it implies additional infrastructures, costs and conversion losses (e.g. chemically with a battery, mechanically by either adiabatic gas pressuring or pumping water back up in a barrage or spinning a flywheel, electrically with capacitors…). The current electrical grid allows international exchange but is not optimal for the highly variable electricity production. However, the smart grid concept being developed is a solution to optimize its transport and consumption, limiting for instance the demand peaks, hence a better match for the renewables.

Ideally, solar cells could be thought of as a main source of electricity for humanity, because the sun always shines somewhere on earth, but are we confident enough in the political stability in the world to rely on an open international network? The human factor may not play in our favor here and the diversity of the energy conversion systems is still an important parameter for an improved resilience; let's only attribute to the solar energy the place it deserves.

### 1.1.3 Industry

This being said, Solar cell industry in Sweden is far from thriving (similarly as in the rest of Europe), manufacturers go bankrupt and are gradually replaced by retailers, question of prices. In Sweden, the large scale commercial activity has been turned off and only 2 manufacturers out of 15 have maintained a minor PV production [d], whereas the national PV installation growth increases exponentially as shown in Figure 3 and Figure 4.

[c] This results include the manufacturing, installation, cabling, the surrounding electronics and the recycling.
[d] *Renewable Sun Energy Sweden AB* (Mono-Si) and *Midsummer AB* (CIGS)

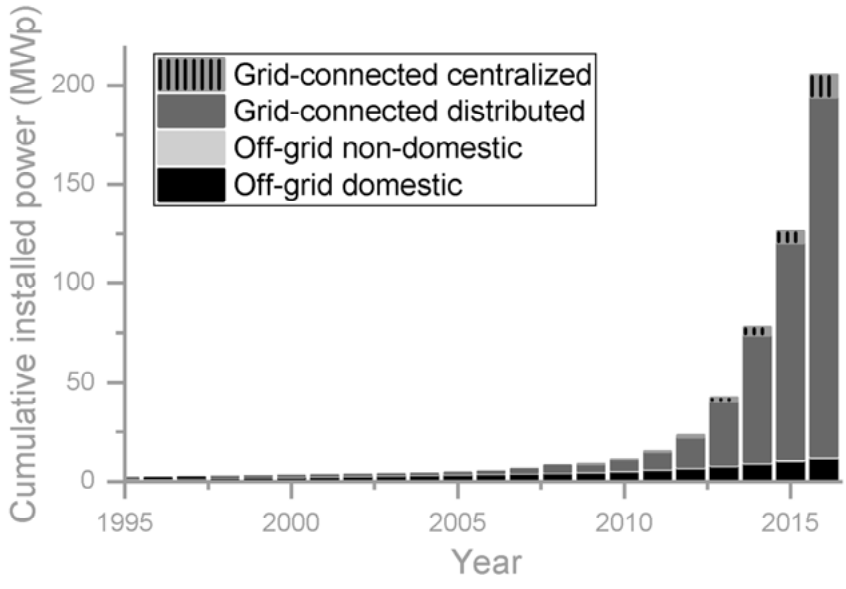


Figure 3 Exponential increase of the installed solar capacity in Sweden between 1995 and 2016. (Data from *the Swedish National survey report 2016*) [7]

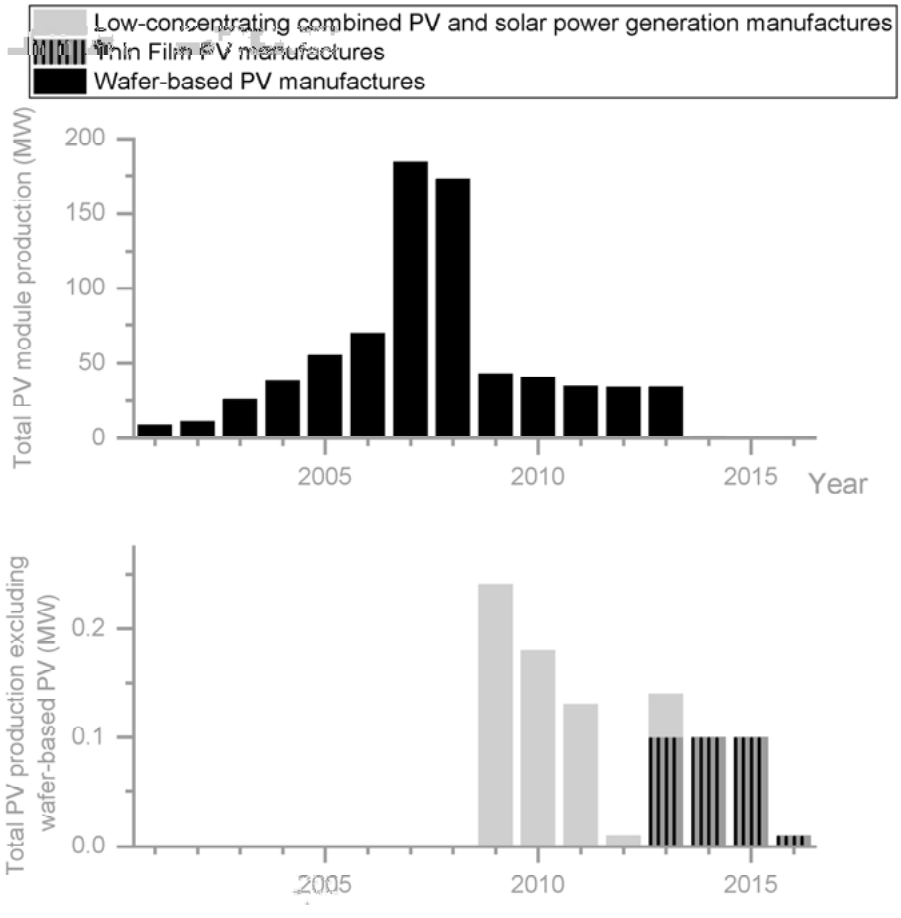


Figure 4 The PV production catastrophe that contrasts with the continuously increasing installation rate. The total PV module production in Sweden between 2000 and 2016 (top), the same figure plotted without the contribution by the wafer-based modules (bottom). The remaining activity is barely visible in these graphs (Data from *the Swedish National survey report 2016*) [7]

### 1.1.4 Thin-film PV

In contrast to silicon-based PV, the thin-film technologies can also reach comparable performances but they require less energy to be manufactured. This leads to a more interesting EROI and EPBT. In addition, the specific thin-film manufacturing can rely on vacuum-based deposition processes or wet-processes too and can be grown on a wide variety of substrates: glass, metals and even polymers. This opens the possibility of employing flexible substrates, quite compatible with larger industrial production (e.g. roll-to-roll process). Among the different thin-films existing, $Cu(InGa)Se_2$ (CIGS) has already demonstrated both a high stability and world-class performances,

competing with polycrystalline silicon technology [8,9]. In addition, their band gap value can be adjusted by simple chemical substitutions.

## 1.2 Key issues

The best lab scale conversion efficiency of a CIGS solar cell is currently around 23% [8], but referring to the theoretical limit of a single junction solar cell, known as the Shockley–Queisser limit, the maximum value should gravitate around 34% (standard test conditions: 25°C, 1000 W/m2, AM1.5) which predicts some room for improvement. Nonetheless the performance always drops when transferring the technology from the lab to an industrial scale as shown in Figure 5, so all the research efforts are not invested in pushing this absolute performance benchmark. Several development strategies rather focus on other parameters that are also essential once out of our labs.

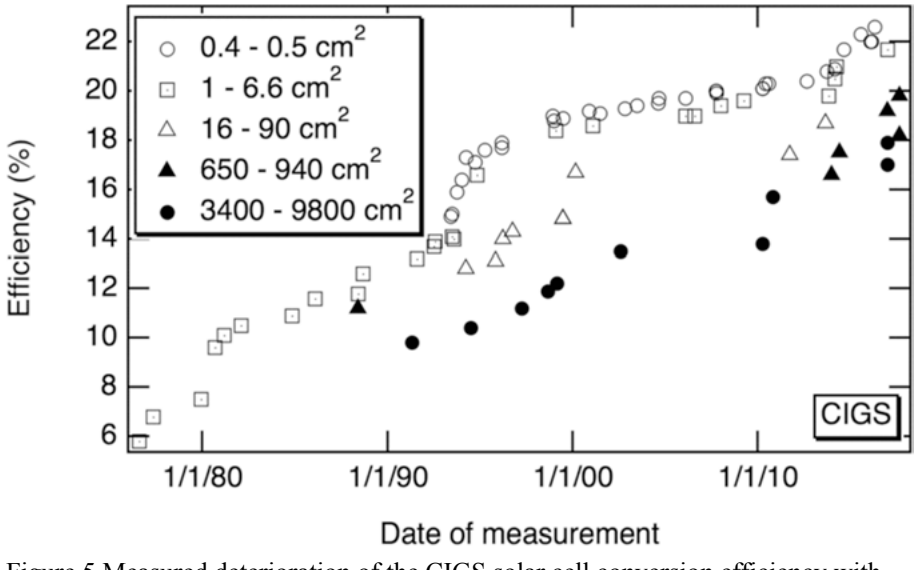


Figure 5 Measured deterioration of the CIGS solar cell conversion efficiency with larger solar cell areas. © [2018] IEEE. Reprinted, with permission, from [Kurtz S, Repins I, Metzger WK, et al. Historical Analysis of Champion Photovoltaic Module Efficiencies. *IEEE J. Photovoltaics* March 2018][10]

The reduction of the weight of the solar cells is a good example, where some roof structures could not sustain the burden of a thin-film using SLG for both the substrate and the encapsulation. The introduction of thin metal or polymer substrates together with composite encapsulation solutions can drastically reduce the total weight [11]. However, steel for instance contains iron which is a serious contaminant for the CIGS absorbers, and measures must be taken to prevent its diffusion. This motivated the study presented in **Paper II** in this thesis.

In another aspect, the control of the interface quality can be a bottleneck for the conversion efficiency. As examples we can cite the cleaning method of the substrates, the surface chemistry of a layer prior to the deposition of the following one (air exposure, *in-situ* sequence, nitrogen storage, wet cleaning, annealing), the pre-sputtering time prior to the actual sputtering, the quality of the vacuum… This non-exhaustive list of examples illustrates the variety and complexity of the parameters that will influence the transport quality of electrical charges through the solar cell stack, hence its efficiency. Therefore, it becomes understandable that transferring a technology from laboratory to industry, probably in a different location, using different machines, equipped with different pumps and targets, requires re-developing a large part of the process. The control of the interfaces is thus an essential research subject in order to improve the performance consistency and to ease technology transfers. Implementation of cleaning steps or intermediate passivation layers are one of the attractive answers to this. Study of an additional passivation layer is the fundament of **Paper I, II III** and **VI**; implementation of intermediary surface treatment is used in **Paper IV** and **V**.

## 1.3 Outline of the thesis

This work is the fruit of collaboration between industry, CRM AC&CS - CRM Group, and academia, the Ångström Laboratory. The underlying ambition was to improve understanding of the CIGS solar cell absorbers with an emphasis sets on interface control, both to enhance scalability (lower thicknesses and wider areas) and to allow transfer to different substrates. As a matter of fact, the interface control is a paramount problem shared by many semiconductor technologies [e]. The first part of this work concerns the study of rear interfaces. In this part, I invested my efforts in understanding the limitations of the diffusion barrier used for steel substrates (**Paper II**). We also enhanced the Mo/CIGS interface quality by developing $Al_2O_3$ rear passivation layer (**Paper I, III and VI**). The second part of this work concerned the control of front interfaces. To do so, the surface chemistry of the CIGS absorber layers was thoroughly analyzed and related to different, sometimes interdependent, deposition process parameters. In **Paper IV**, I extensively studied potassium induced modifications of CIGS absorbers, providing KF either during the co-evaporation growth or during a Post Deposition Treatment, or both. In **Paper V**, silver-alloyed CIGS (ACIGS) was introduced and studied. I investigated ACIGS chemical and structural modifications induced by KF-PDT, highlighting the existence of process window limits beyond which the treatment becomes quite detrimental.

[e] C.f. the Nobel prize in Physics 2014, for the achievement of an efficient blue LED, which has allowed the emergence of all of our current white LEDs.

# 2 Physics of Semiconductors

*Foreword*

Let's not try to reinvent the wheel. The underlying physics of semiconductors is well known and already described in different good reference books [12–14]. The ambition of this part is to help a neophyte [f] to understand the concerns of semiconductor physics, and hopefully to trigger the appetite of reading more about it. However, the experienced reader should not be left aside and will be pleased to find a comprehensive summary of semiconductor materials and of the measurement techniques used during this work.

## 2.1 What a semiconductor is

We ought to start from the beginning. We know what a conductor and an insulator is, the former can transports an electrical current but the latter generally blocks it. Filling the gap between these two categories are the semiconductors. The usual way of defining them more accurately is sketching their electronic structure as in Figure 6. Electron occupancy for insulators will be restrained to the valence band, where electrons are strongly bonded to the atoms. The presence of a wide energy gap to the conduction band level hardly allows them get excited and wander the neighborhood, or in other words, to move from their atom to the next one. In contrast, a conductor electronic structure contains many electrons in the conduction band which are delocalized and free to move across the material thus can conduct a current. Semiconductors can be everything in between. Usually, they only have a few electrons in the conduction band but the energy band gap from the valence band to the conduction one is small enough to be crossed, switching it from fair insulator to fair conductor. The energy necessary to excite an electron and make it cross the band gap may be provided by heat (e.g. increasing from 0 K to room temperature), visible light or other electromagnetic radiations. Then, we already foresee that the boundaries separating conductor/semiconductor and semiconductor/insulator can be quite situational, depending for instance on the application device temperature. Furthermore, the electron occupancy is defined by the Fermi level, but the Fermi level position can be tuned by modifying the doping level [12,14]. This offers an in-

[f] From the greek *Neophutos*: "Newly planted"

teresting lever to adjust the conductivity of a semiconductor closer to what is needed.

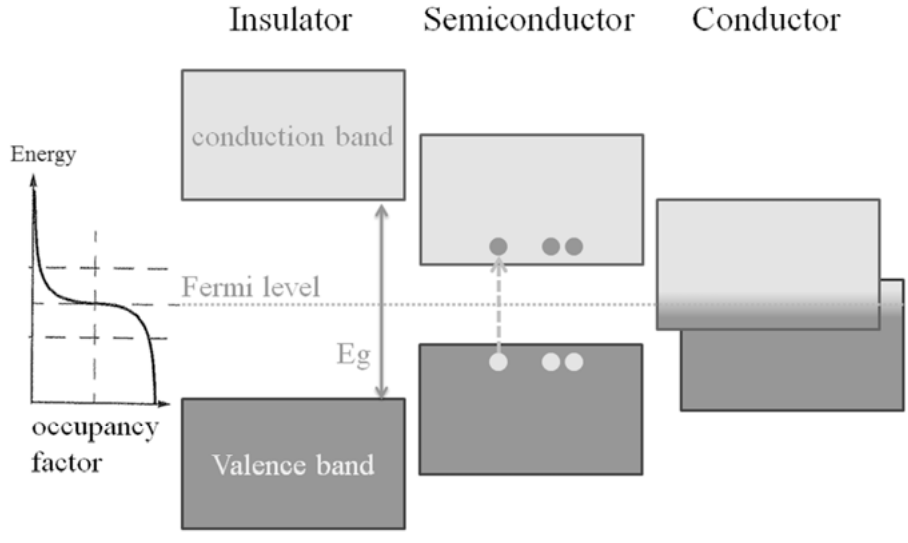


Figure 6 Energy band structures schematic representing insulator, semiconductor and conductor material. Insulators typically have no free charge carriers, semiconductors have temporary electron-hole pairs that can be generated to transport a current, and conductors natively have free charge carriers.

## 2.2 Photovoltaic effect

The use of the photovoltaic principle is really old as it appeared with the chlorophyll from Cyanobacteria about 2.4 billion years ago [15]. In their case, the electric charges are directly converted to chemical energy. The first human observation of a photo-induced current was made in 1839 by Edmond Becquerel, but it's only from the middle of the 20th century that industry, the Bell Laboratory as pioneer, kicked in and exploited this discovery. Since then, research was dedicated to improve the conversion efficiency by assessing new materials, developing the deposition processes, and understanding the origin of losses to mitigate them [6,16]. With this thesis, I have pursued the development of one specific thin-film absorber material, the chalcopyrite $CuInSe_2$ family.

When photons encounter a semiconductor material, they can, if their energy is larger than the band gap separating the valence band from the conduction band level, excite an electron from its valence band position and generate a so-called electron-hole pair. In any semiconductor under illumination[g], this

[g] Given that the radiation energy is greater than the band gap value.

charge carrier generation occurs continuously and is referred as *the generation rate*. Once created, these charge carriers may randomly encounter each other and recombine (*the recombination rate*). T*he charge carrier lifetime* is the average time between generation and recombination for a charge carrier and a long minority carrier lifetime is essential for high solar to electric power conversion efficiency. The recombination is called radiative when a photon is emitted, and non-radiative when it only generates phonons as for the trap-assisted and Auger recombinations as featured in Figure 7 [12]. The goal for us is to obtain a charge carrier lifetime long enough to collect them at the contact and only let them recombine after having been transported through an external circuit, generating the desired photocurrent.

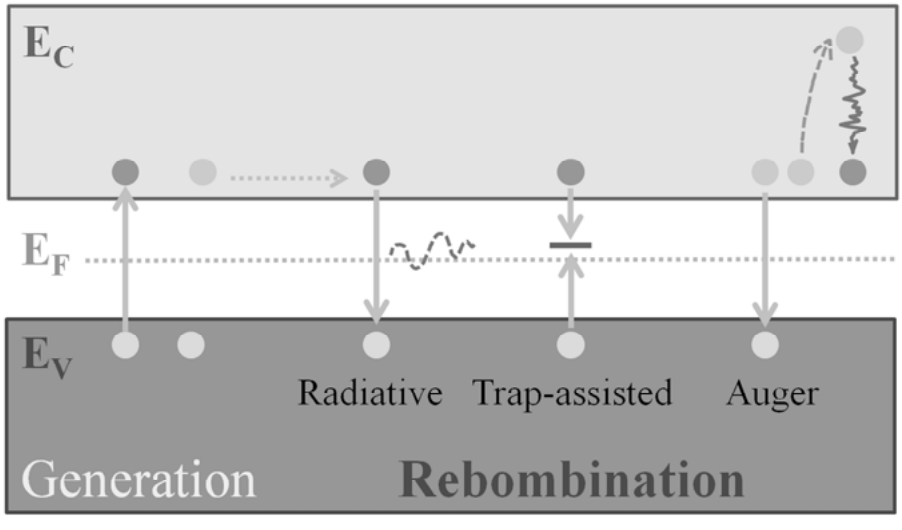


Figure 7 Sketch of the different recombination mechanisms. The trap-assisted and Auger recombination are non-radiative recombination.

## 2.3 PN junction

The PN-junction is this one-way charge sorting portal. It consists in the assembly of two oppositely doped semiconductors, one n and one p. Once in contact, the nearby mobile charge carriers cancel each other forming a depletion region, leaving only the fixed charges of the ionized dopants in place, positive on the n-side and negative on the p-side. These fixed charges generate an internal electric field that will further drive opposite charge carriers in opposite direction, creating a *drift current*. This junction may be defined either as a homojunction if the same semi-conductor is used (e.g. Si:n and Si:p), or as a heterojunction if two different materials are used (e.g. CIGS(p) and CdS(n)). For both cases, the quality of the PN interface is paramount for the device properties.

## 2.4 Solar cell structure

A solar cell is a combination of a photon absorber and a PN-junction, to generate and separate charge carriers. On each side of this assembly, a front and a rear contact is added to transport the charge carriers to the external circuit, as wires would do in a battery. The contacts need to feature a good conductivity, but there are some extra essential requirements:

- The front contact has to be as transparent as possible to the collected wavelength otherwise no light would reach the absorber layer (simple things that might ruin an entire project)
- The energy band offsets ($\Delta E_c$ and $\Delta E_v$) between the contacts and the semiconductor have to be optimized to limit the charge recombination at the interfaces [17].

It is therefore quite usual to use a metal as a back contact to provide a high conductivity, and a transparent conductive oxide (TCO) as a front contact to find a balance between the transparency and conductivity parameters. Additional metallic fingers (e.g. Ni/Al/Ni) usually assist the front contact performance, bringing some shadowing but enhancing the global conductance as sketched in Figure 8.

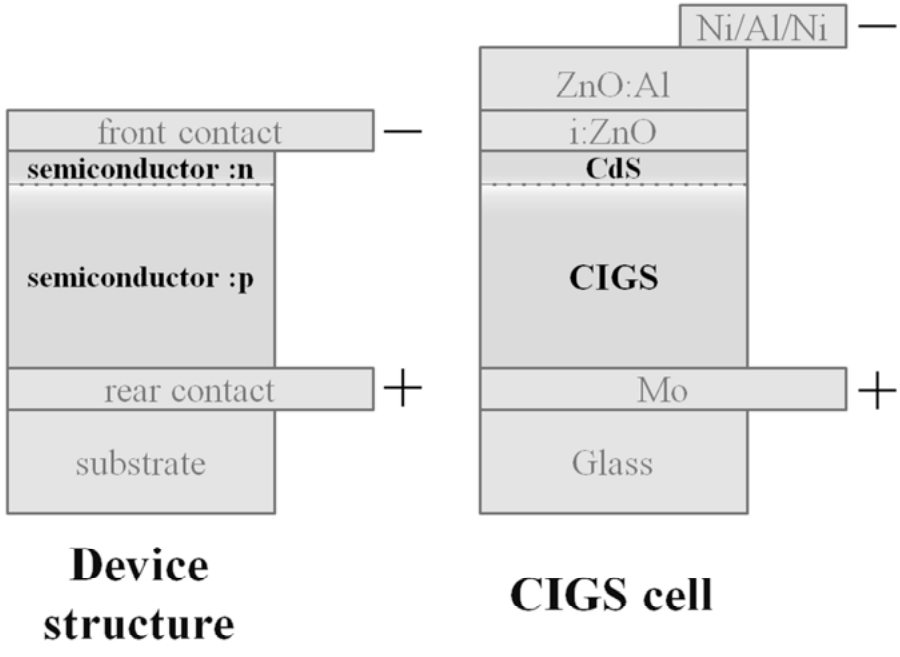


Figure 8 Possible structure of a solar cell (left) and regular structure for a CIGS thin film solar cell. Note that other stacking configurations are also used.

One major concern though is the conduction band alignment of the different layers. For a metallic back contact, it is of great significance to choose a metal with an appropriate work function ($\phi$) in regard to both the electron affinity ($\chi$) and work function ($\phi$) of the semiconductor to minimize the Schottky barrier spontaneously formed at the junction of the two and generate an ohmic contact [14]. Concerning the TCO material, its electron affinity ($\chi$) has to match the one of the semiconductor to reduce the conduction band offset and its doping has to be tuned specifically to enhance the current flow as illustrated in Figure 9.

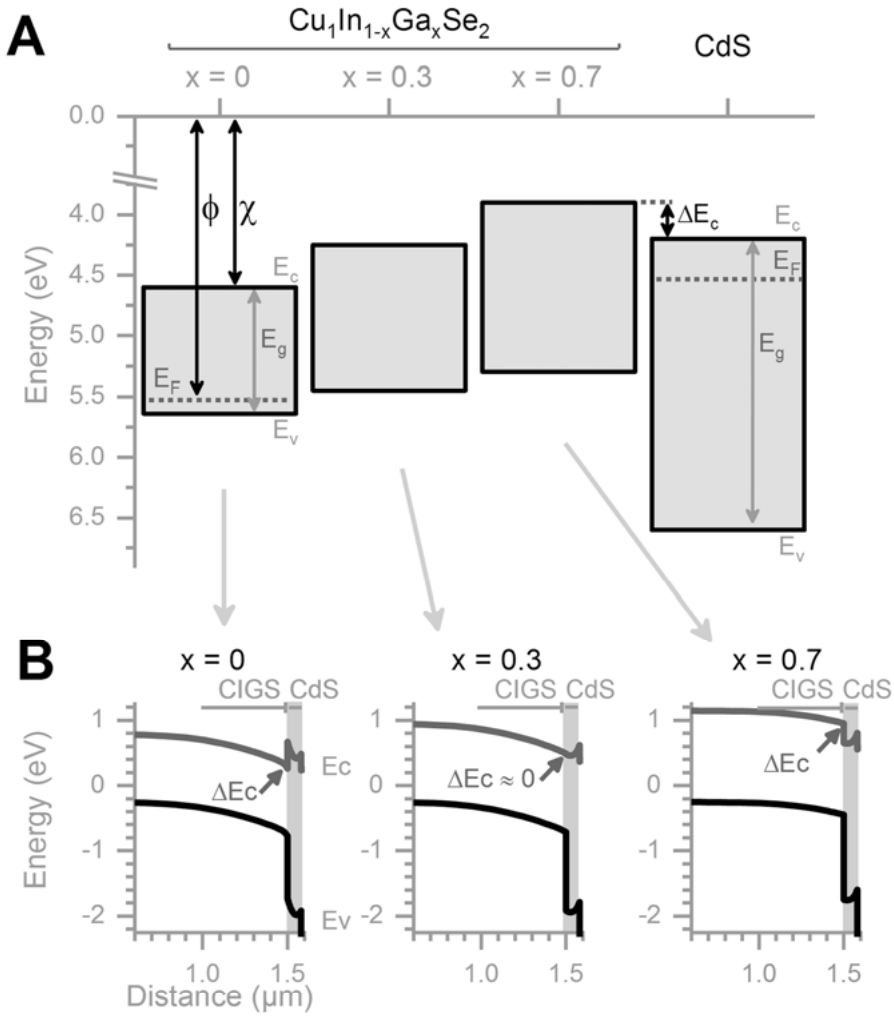


Figure 9 CIGS/CdS heterojunction energy band diagrams before contact (A) and in contact (B) simulated with the Solar Cell Capacitance Simulator (SCAPS) [18]. The CIGS conduction band position depends on the Ga/(Ga+In) ratio and can show an offset ($\Delta E_c$) in regard to the CdS conduction band (A). The different conduction band offsets result in either a spike or a cliff in the conduction band, both potentially detrimental for the electron flow. The presence of a spike is a barrier for the electrons to go through, and the cliff induces a reduction of the internal electric field (B).

Besides these fundamental physical restrictions, additional criteria also need to be accounted for. Indeed, one must consider the possible reactivity of the contacts with the semiconductor during the deposition process [h], their long term stability, optical properties, price, toxicity and so on. This non-

[h] This is the reason for the Ni/Al/Ni stack used as the metallic fingers. Using only Al would rapidly oxidize from the ZnO oxygen content and block the current flow.

exhaustive checkup list explains partly the usual hassle to identify a better candidate material to replace an existing one.

## 2.5 Solar cell absorbers

Let's now detail what semiconductors make interesting solar cells absorbers. The candidate has to show both a stable structure, an efficient optical absorption around the visible light spectrum and good electrical properties.

The stability is necessary to easily manufacture the material but also to not see it degrading over time. An increased optical absorption, as for using direct band gap material instead of indirect ones, allows reducing the thickness of the absorber layer [i], hence a lowered material consumption and lower demands on electronic material quality. The electrical performance, namely the charge carrier diffusion speed, diffusion length and carrier lifetime or even the carrier recombination rate define how far charge carriers can travel before recombining. Maximizing those parameters would indeed increase the probability for a charge carrier to cross the PN junction (and contribute to the photo-current), hence lowering the electrical losses. A large amount of the interesting candidates actually gravitates around the group IV of the periodic table, leading to an average of 4 valence electrons like Si (IV), CdTe (II-VI), GaAs or InP (III-V) and our CuInSe2 (I-III-$VI_2$). The variety is explained by the fact that each of them has strengths and weaknesses and performs better in specific applications. Many more combinations are expected to lead to viable semiconductor materials and are still in the research states.

## 2.6 Conversion losses

If we wish to discuss efficiency of a solar cell device, then we must describe the different losses. They can be sorted out in two categories, the optical losses and the electrical ones.

### 2.6.1 Optical losses

Part of the optical losses are caused by light reflection and absorption that occur before the light enters the absorber layer, the place where the absorbed light can generate photon-induced carriers which contribute to the photo-current. Most common solutions to minimize the losses employ anti-reflective coatings (interference or texture) and wider band gap materials for the front transparent part of the solar cell, limiting thereby the blue wave-

[i] The absorption coefficient of CIGS is approximately 2 orders of magnitude higher than silicon, which allows the absorber to be 100 times thinner maintaining the full absorption [97]

length parasitic absorption. Another part is linked to the band gap energy. Photons of energy lower than the band gap ($E_g$) of the semiconductor cannot be absorbed and are lost. They are absorbed if their energy is equal to or higher than the $E_g$. But there is a catch, since the excess of energy higher than $E_g$ is lost by thermalization process, i.e. heat loss. Therefore, a solar cell made from a semiconductor with a relatively small $E_g$ value can absorb a large part of the solar spectrum, but displays higher thermalization loss compared to its counterpart with a large $E_g$, which is transparent to photons of low energy, but has lower thermalization losses for the higher energy photons which are absorbed. The multi-junction solar cells (e.g. tandem structure) directly benefit from lowering these losses [19]. The Shockley-Queisser (S-Q) limit relates the theoretical maximal efficiency ($\eta$) to the energy band gap $E_g$ for a single junction solar cell. With a band gap tunable from about 1 to 1.7 eV, the CIGS absorber material can be adjusted to optimal theoretical values, avoiding the ranges of strong atmospheric absorption (cf. Figure 10 and Figure 11).

One reference parameter often displayed is the so-called voltage deficit, which is basically the difference between the voltage predicted by the S-Q limit and the measured open-circuit voltage. The deficit is usually several hundreds of millivolts, but increases with higher non-radiative recombination rate (cf. Figure 10).

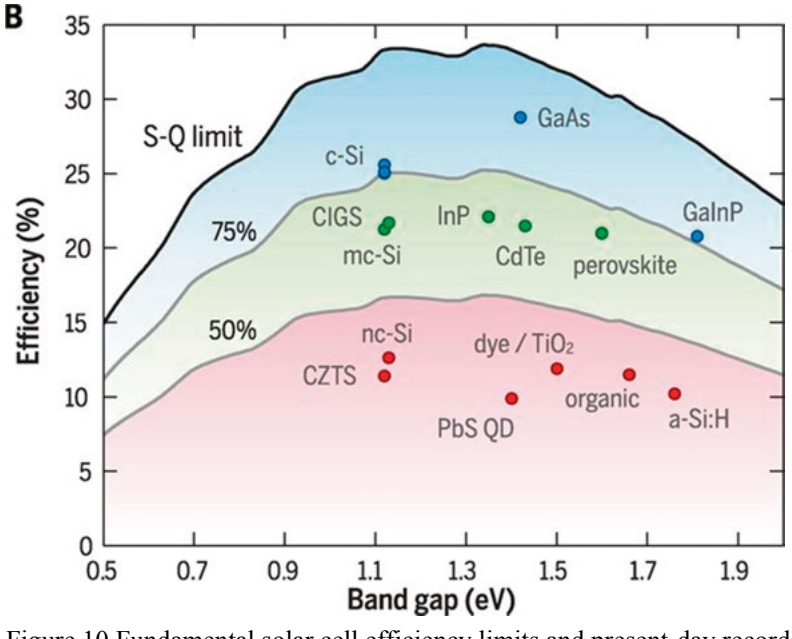


Figure 10 Fundamental solar cell efficiency limits and present-day records (2016). Theoretical Shockley-Queisser (S-Q) detailed-balance efficiency limit as a function of band gap (black line) and 75% and 50% of the limit (gray lines).The record efficiencies for different materials are plotted for the corresponding band gaps [20]

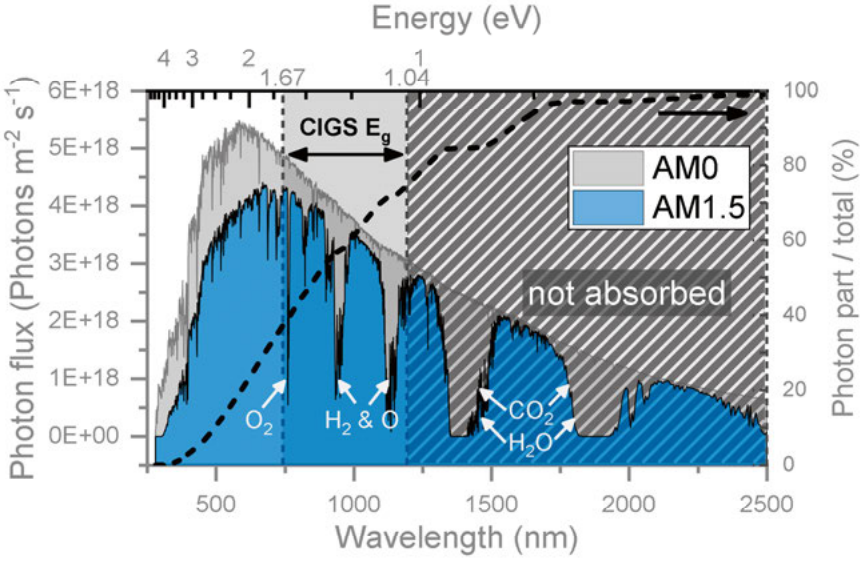


Figure 11 Photon flux of the solar spectrum. AM0 is the extraterrestrial spectrum and AM1.5 corresponds to the solar spectrum as received on a 37° tilted surface facing the sun. The grey rectangle symbolizes the accessible band gap values for CIGS semiconductor, around the optimal band gap value as predicted by the Shockley-Queisser limit. The right y-axis shows the fraction of the solar spectrum that can be collected using different band gap values (data from ASTM International [21]).

### 2.6.2 Electrical losses

Electrical losses are related to the joule effect and the charge carrier recombination. The recombination rate is a function of crystal defects, dangling bonds or impurities, and as mentioned previously, contributes to the voltage deficit. In this work, the emphasis was set on limiting the carrier recombination rate occurring at the interfaces of the absorber layer, usually referred to as interfacial recombination or trap-assisted recombination.

For CIGS material, reports indicate that the voltage deficit increases with the band-gap values (or higher Ga content) [22], therefore the cells do not reach the predicted open-circuit voltage and tend to see their Voc saturating, consequently limiting their conversion efficiency (Figure 12). The introduction of alkali-metal Post-Deposition Treatment (PDT) which has been shaking CIGS development for several years and permitted all the recent conversion efficiency records, allowed shifting the Voc saturation up to higher band gap values as described in the following section (cf. Figure 13). In a related topic, partial substitution of copper by silver was also reported to reduce the voltage deficit, resulting in a higher Voc at similar band gap values (cf. Figure 14).

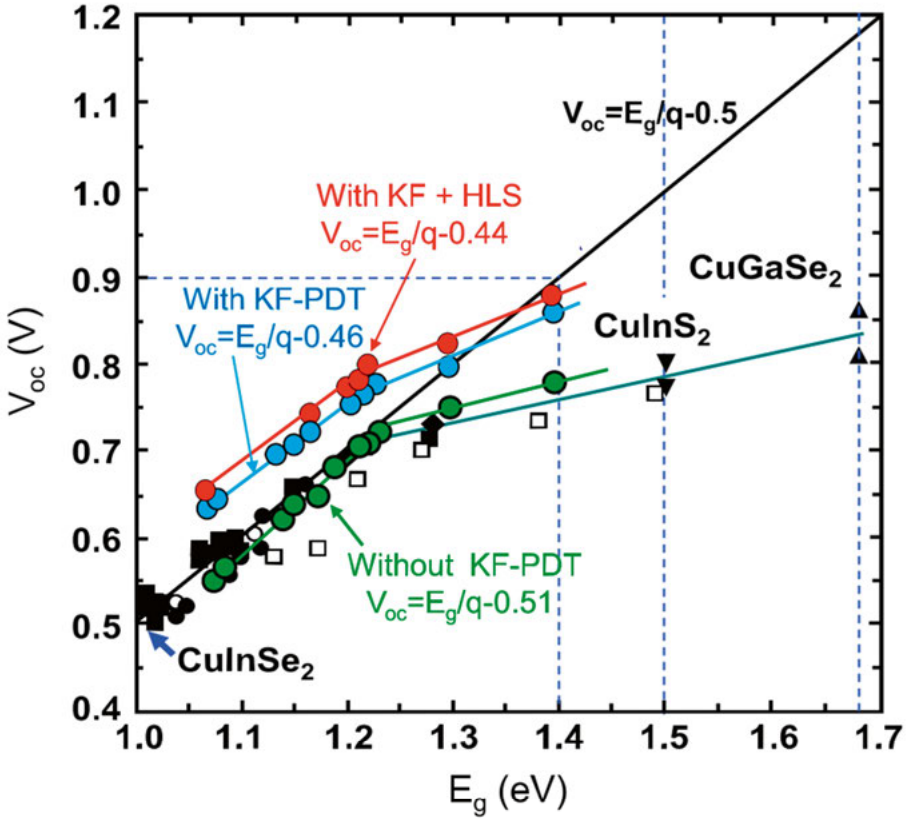


Figure 12 $V_{oc}$ of KF-treated CIGS solar cells before (blue circles) and after heat-light soaking (HLS) (red circles) as a function of Eg. For comparison, the $V_{oc}$ of KF-free CIGS solar cells (green circles) of the same batches are also plotted over the data presented by Herberholz et al. [22,23] The heat-light soaking effect will not be discussed in this thesis.

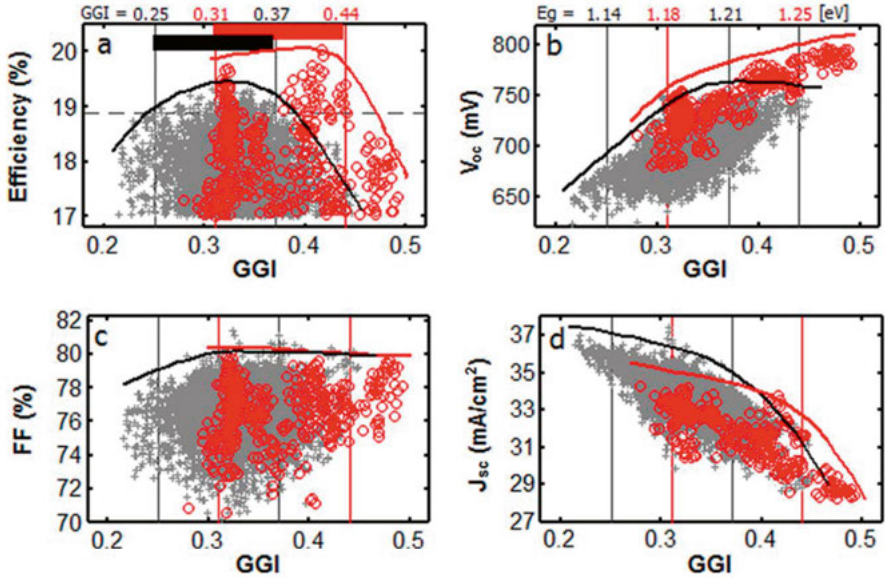


Figure 13 Comparison of cells with $\eta \geq 17.0\%$ (without ARC): group A (grey crosses/n(w/o KF) = 6936) represents cells without KF and group B (red open circles/n(KF) = 437) cells with KF post-treatment. The KF treatment enables the extension of the high efficiency corridor in which Voc follows the increase in GGI without saturation [24]

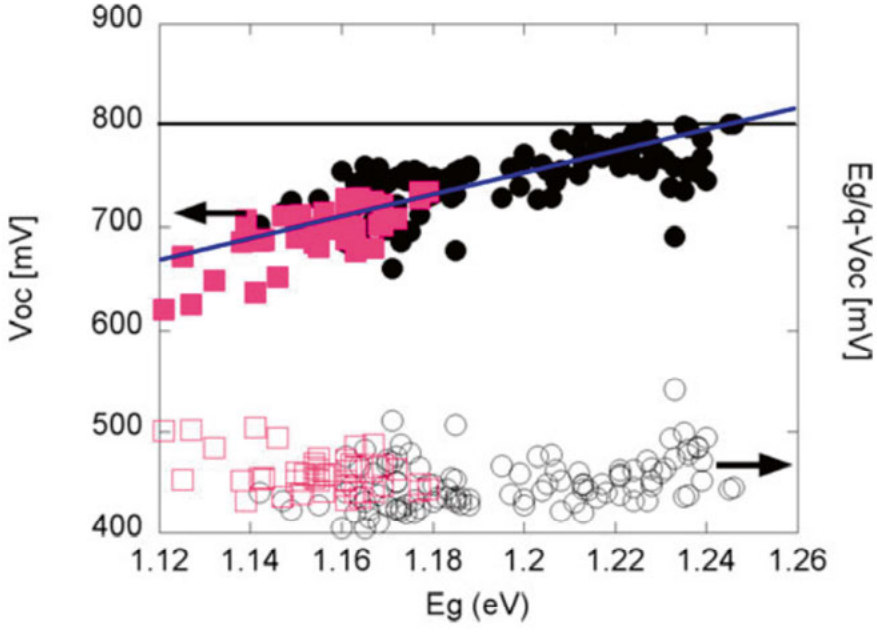


Figure 14 Voc versus Eg (left axis, filled symbols) and voltage loss Eg/q − Voc (right axis, open symbols) for a collection of ACIGS and CIGS cells. Black symbols:ACIGS, magenta symbols: CIGS. The average voltage loss is 449mV for ACIGS (minimum value: 405) and 460 mV in average for the CIGS devices (minimum value: 432). The blue line corresponds to a voltage increase equal to the bandgap increase (no additional voltage loss) and is added as a guide to the eye © [2017] IEEE. Reprinted, with permission, from [Edoff M, Jarmar T, Nilsson NS, et al. High $V_{oc}$ in (Cu,Ag)(In,Ga)Se 2 Solar Cells. IEEE J. Photovoltaics Nov. 2017] [25]

## 2.7 Electronic defects and passivation strategies

### 2.7.1 Impurities

Steel substrates can be used for a CIGS roll-to-roll deposition process [26,27] and the thermal expansion coefficients can be similar, which reduces extrinsic stress. But from a chemical point of view, the two are not a good match. Metallic ions out-diffuse from the substrate into the CIGS during the high temperature co-evaporation, adding many impurities into the fresh absorber layer. Problems arise when impurities are electronically active (donor-like or acceptor-like defects), adding electronic states within the semiconductor band gap. Indeed, such gap states enhance the trap-assisted recombination rate that reduces the electrical performance of the semiconductor. Considering that the recombination rate (U) is essentially governed by the traps located close to the mid-gap, one can estimate it using the relation:

$$U = \frac{\sigma_n \sigma_p \upsilon_{th} N_t (pn - n_i^2)}{\sigma_n (n + n_i) + \sigma_p (p + n_i)}$$

Where $N_t$ is the trap density, $\upsilon_{th}$ is the thermal velocity and $\sigma_n$ and $\sigma_p$ are the capture cross sections for electron and hole, respectively [12].

While Fe and Ni are reported to be the most detrimental impurities for CIGS, only Fe seems sufficiently mobile to reach the absorber layer. Cr is also observed to diffuse easily but does not seem as detrimental as Fe [28]. The amount of impurities required to deteriorate the performance is fairly low, below 20 ppm for Fe [29] Presence of iron is believed to increase the carrier recombination rate through $Fe_{In}^{2+}$ (or $Fe_{Ga}^{2+}$) deep acceptor states and to alter the p-doping of the absorber layer because of the $Fe_{Cu}$ substitution defects [30,31].

*Barrier: Blocking the diffusion*

To prevent the detrimental contamination of the absorber layer, most of the groups employing steel substrates implements a thick dielectric barrier on it from 1 µm to 130 µm [32–35] or metallic barriers from 60 to 200 nm [36], sometimes in addition to a reduced deposition process temperature to slow down the diffusion [37].

### 2.7.2 Structural defects

Absorber layer crystallization occurs with a certain degree of disorder. For instance, In or Ga atoms may settle where a Cu atom is expected, forming $In_{Cu}$ ($Ga_{Cu}$) anti-site defects. But because their valence is dissimilar to Cu they act as electric defects. From theory (Lany and Zunger), the antisite defects appear in combination with Cu vacancies in Cu-poor material, where the defect complex ($2V_{Cu}$+$In_{Cu}$) is neutral. A Cu-poor CIGS material can accommodate many of these defect complexes, making the material tolerant to compositional variations. The $V_{Cu}$ is a shallow acceptor and is the major source of p-doping in CIGS [38,39]

In addition, the transition from one layer to another (especially without epitaxial growth) or at the transition from one crystal to another in polycrystalline material, can leave structural defects (e.g. selenium vacancies and other dangling bonds) [40]. Improving the process is the prime way to enhance the material quality and different levers like the deposition speed, temperature or the process pressure can be used for this. However, it is often more complicated than solely turning one knob, so alternative approaches have been developed to reduce the defect formation or limit their influence.

**a. Ag-alloying:**

Silver-alloying of the CIGS is reported for lowering both the melting temperature and the crystal disorder [41]. The alloying also displays a slight effect on the band gap value [42] and reduces the voltage deficit [25,43]. This improvement may be attributed to the band gap widening that would actually shift the conduction and valence bands downwards, maintaining a low conduction band offset (CBO, $\Delta E_c$) with the CdS buffer layer [44–47]. The Ag/(Ag+Cu) ratio (Ag/I) can vary from 0 to 1, but seems to reach an optimum around 0.2-0.3 for the electrical characteristics of the devices [46]. In our process, silver was co-evaporated with the other metals.

**b. Alkali-metals**

Addition of alkali metals has a significant influence on the cell performance and it can be done in several ways [48]:

- out-diffusion from an alkali-containing substrate (e.g. SLG, Mo:Na)
- using a precursor layer (e.g. NaF)
- co-evaporating alkali-metal during the CIGS growth
- Performing a PDT once the CIGS growth is finished

The addition of alkali-metal is reported to passivate the donor-like defects of the absorber layer [49,50], to improve the surface potential homogeneity [51,52], and to passivate the $V_{Se}$ [53,54]. As a result the processed devices exhibit lower voltage deficits, higher Voc and higher efficiencies.

The addition of Na may increase the doping of the CIGS layer several orders of magnitude, by increasing the number of $V_{Cu}$. This leads to a higher separation of the quasi-Fermi levels and thus the output voltage of the CIGS solar cells.

**c. Surface field passivation**

If interfaces are nests for defects, one approach consists in keeping the minority charge carriers away from them. There are different ways to achieve a field passivation. First, the absorber band gap can be graded to be wider close to the interfaces. This way charge carriers are be invited to stay in the bulk of the absorber where the recombination rate is lesser. For CIGS materials, the Ga/(Ga+In) ratio defining the band gap [55] is regularly graded for this reason [56]. The different PDT treatments using sulfur or alkali-metals induce shallow surface modifications that increase the band gap over a few nanometers close to the front surface, inducing a field effect passivation [57,58]. Alternatively, an oxide layer containing fixed charges can be interlayered below or above the absorber layer. For CIGS an $Al_2O_3$ oxide layer was reported to contain fixed negative charges repelling the minority charge carriers away from the rear interface. [59]

# 3 Characterization techniques

## 3.1 The field of electron microscopy

Most of us are familiar with microscopy, but not as many are with electron-microscopy. The electron-microscopy is really a whole world quite different from light microscopy, based on electrons instead of photons. This section will describe how electrons can be used to probe the matter, and the working principles of the main techniques used during this thesis.

*Why electrons instead of photons?*

The original reason was to overcome the resolution limit of light microscopy, restrained by the illumination wavelength as described by the Rayleigh criterion [60]. Using electrons already pushed the resolution below the atomic scale to approximately 0.1 nm, many orders of magnitude better than with visible light. Despite this performance, improvements are still expected because the predominant limiting factor is the aberrations from the electromagnetic lenses.

A second reason for using electrons is related to electron-matter interaction. The close interaction between the fast electrons from the beam and the sample can release many different measureable elements of distinct physical origins, thus offer various interesting pieces of information. To describe these interactions, we usually divide them into two categories: elastic and inelastic interactions.

Elastic interactions occur with nearly no energy transfer, as for example when the fast electrons are scattered by the coulomb interaction with the sample atom nuclei (Bremsstrahlung radiations aside). The main applications of elastic scattering are the Bright-Field (BF) and Dark-Field (DF) imaging modes and the subsequent diffraction techniques.

Inelastic interactions involve an energy transfer from the fast electrons to the atoms of the sample, as observed for example with ionization phenomenon or the Bremsstrahlung radiations ("braking" radiations). They generate several particles like photons, Auger or secondary electrons. A second aspect of the inelastic interactions involves the matter as a whole and not only as individual atoms. In a semiconductor, the fast electrons can induce band-to-band transitions and generate electron-hole pairs as described in the previous section. These charge carriers can induce a current that we are able to meas-

ure with the Electron-beam induced current (EBIC) technique. Besides, the charge carrier recombination can also generate photons that are collected with the cathodoluminescence techniques. Finally, the fast electrons may excite collective ordered oscillations originating from the electron density or from the crystal lattice which release plasmon and phonons, respectively.

The Electron Energy Loss Spectroscopy (EELS) is a product of all the elastic and inelastic scattering events, whereas the Energy Dispersive X-ray Spectroscopy (EDS) is exclusively scrutinizing the X-rays emitted during the relaxation of the excited atoms (and from the Bremsstrahlung radiations).

Overall, the major strength of electron microscopy is probably its capability of delivering information about both the structure and the chemistry of a sample, with a lateral resolution potentially better than the interatomic distances of most materials.

## 3.2 Transmission Electron Microscopy (TEM)

The discovery of the electron was made in 1897 by J.J. Thompson and only 30 years later, in 1931, Max Knoll and Ernst Ruska finished building the first TEM instrument. However the first commercial versions were only available in the early 40s.

Since then the tools are in constant evolution, the vacuum quality was improved, field-emission guns replaced the thermionic electron sources, the photographic plates used to record the signals are now digital Charge-Coupled Device (CCD) sensors, sample holders display a higher stability and control, and more recently the implementation of chromatic and spherical aberration correctors expanded again the existing resolution limitations [61]. The latest evolutions concern, among other things, the introduction of direct detection cameras.

**a. Instrument architecture**

While a detailed schematic of the microscope would be inappropriate for this introduction, I deem necessary to sketch the TEM architecture to ease the understanding. The electrons are charged particles so their trajectory can be altered using magnetic fields (i.e. the Lorentz forces). Each part of the microscope contains group(s) of lenses, where each lens can be quadrupole, sextupole or even higher depending on the needs.

The electrons are generated by the electron gun and accelerated using a fairly high tension, usually ranging from 80 to 300 kV. The beam is then shaped by a condenser system and directed onto the sample. The sample, which was prepared to become electron transparent, is mounted in a holder that can tilt and move along different axes.

The objective lens is the central eye of the microscope. It generates both the first image of the sample (in the image plane) and its associated diffrac-

tion pattern (DP) (in the back-focal plane). From there, the projector system magnifies this image (or the DP) from its original 50x to up to a million times, and projects it to the screen (phosphorous screen or digital camera) (cf. Figure 15).

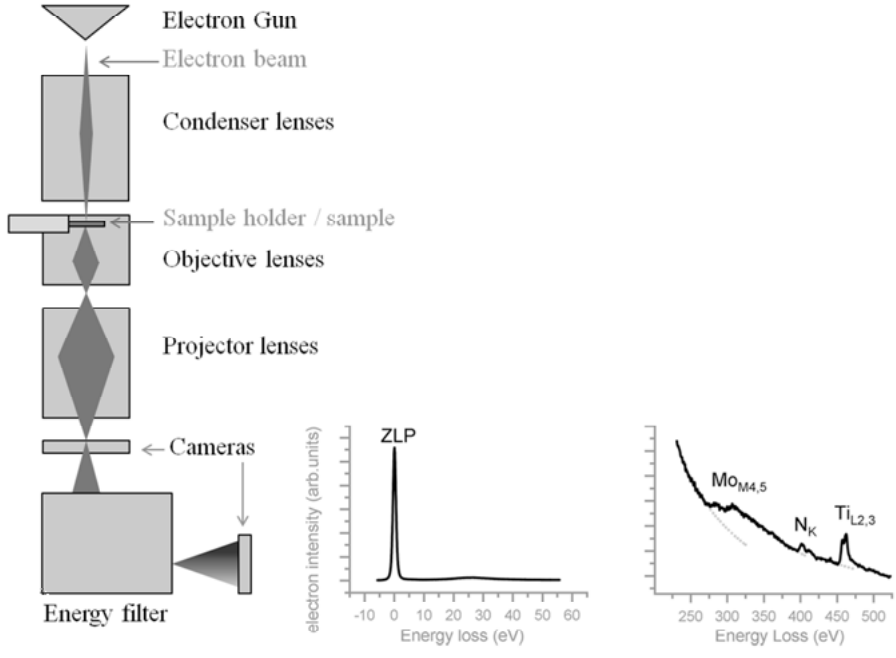


Figure 15 Simplified sketch of the TEM instrument. The two plots feature a typical low-loss spectrum with the main contribution of the Zero loss peak (left) and a core-loss spectrum containing characteristic ionization edges of Mo, N and Ti (right). The sample is actually a TiN layer deposition on a Mo layer, which makes sense.

**b. Working principle of a TEM**

Let's now discuss about the concrete use of an electron microscope. We distinguish two modes. The easiest mode to understand is the parallel beam illumination as it resembles light microscopy. The parallel beam goes through a transparent sample and we observe a shadow image, i.e. the BF and DF images. The image contrast is enhanced by selectively exclude (or include) a part of the scattered electrons to form the image.

The second mode, scanning, is less intuitive but equally important if not more. In this mode the beam is focused on the sample, similarly as when using a magnifying glass to burn ants, and scanned by step across the surface as drawn in Figure 16. We then record the scattered or/and transmitted signal intensity at each step to create a pixel-based image of the surface. More intuitively, if an ant wanders on a transparent glass slide far above the ground, our eyes would perceive an intense scattered light if the probe were placed on the poor insect but a much weaker one if placed on the transparent support (cf. scattered light signal). On the contrary, the directly transmitted light

as shown in the example would be the most intense when only going through the glass and much weaker when obstructed by the ant. In a TEM, this artificial image can be generated by collecting for instance the transmitted electrons (bright-field detector (BF)) or the diffracted ones (dark-field detector (DF), annular DF (ADF), high angle ADF (HAADF). In electron microscopy though, the interaction with matter leads to a large number of signals to record as described above. Hence, in each of the recorded pixel we can store an additional EDS and EELS spectrum (or both). Doing so, we generate a so-called 3D dataset where the first 2 dimensions are the image of the area and the third one is the energy spectrum.

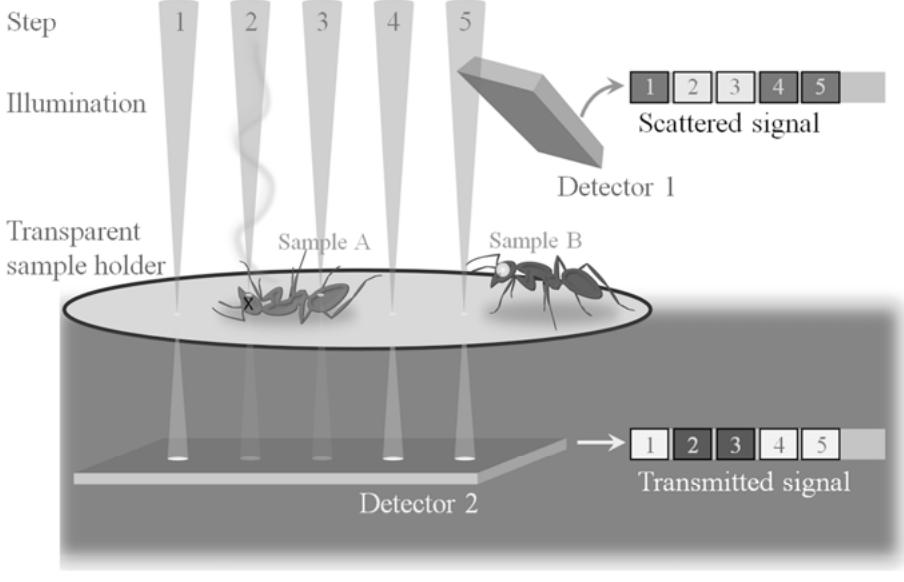


Figure 16 Drawing detailing the principle of the scanning mode. Each pixel is recorded sequentially, one at the time. The example illustrates the parallel reconstruction of one line of pixels based on the light received by two different detectors. Note that the scattered light could also be collected from below the transparent support.

To record a transmitted signal though, the sample must be electron transparent, thus around 100 nm in thickness for many material [62]. Referring to the previous example in Figure 16, if the ant is opaque the transmitted signal is solely binary, either blocked or transmitted. However, if the insect is translucent, the transmitted signal will contains numerous shades of grey offering information about the thickness of the insect or its internal structure. This implies that the sample to be observed has to be thinned, hence prepared, which can damage it. In addition, the size of a TEM lamella is restrained to a few micrometers for preparation related matters, so the candidate area must be selected wisely to be representative of the original sample.

## 3.3 Electron Energy Loss Spectroscopy (EELS)

### 3.3.1 Principle

While all the elastic and inelastic interactions contribute to the energy loss spectrum, the specific inner-shell ionization losses were the most interesting for my analyses, hence my detailed description of it.

An inner-shell ionization event occurs when a fast electron transfers enough energy to a core electron of the sample and excites it from its energy shell to a higher energy state [j]. The ionization energies are characteristic of each element, so by measuring the energy lost by the fast electrons after they have travelled through the sample, we can reconstruct the chemical signatures of the chemical components present in our sample as featured in Figure 17. The specific shapes of the ionization edges, the Electron energy loss near-edge structure (ELNES) technique, may also be of interest as it can contain information about the density of states of the scanned elements, (e.g. chemical bonds).

[j] e.g. K, L, M as described by the Bohr atomic model [63]

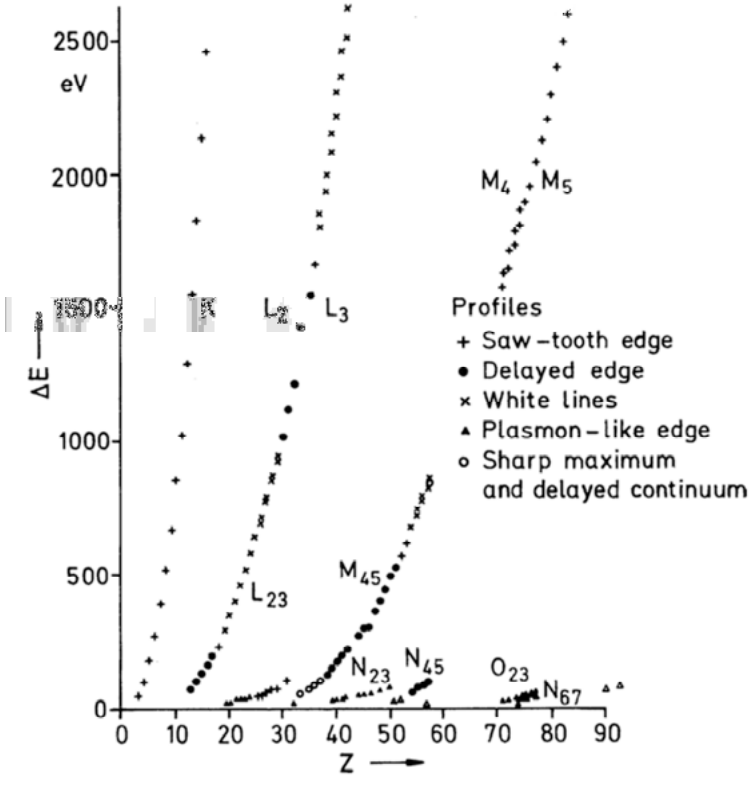


Figure 17 Position of the ionization edges within the energy-loss interval ΔE = 0–2.5 keV as a function of the atomic number [63]

In practical applications, the fast electrons are accelerated to a high energy with a well-controlled spread (e.g. 300 keV nominal energy (way beyond typical ionization energies) with ± 1 eV energy spread for the Tecnai F30ST from FEI), directed through the lamella and sent in an energy filter which spatially distributes the electrons in function of their energy. This allows building a spectrum with, on one side a large Zero Loss Peak (ZLP), corresponding to the fast electrons going through the sample avoiding significant inelastic interactions, then some plasmon losses and the characteristic ionization edges with increasing energy loss. Typical spectra are plotted in Figure 15.

### 3.3.2 Quantification

Quantification of elements e.g. across interfaces is essential to gain understanding of their properties. Therefore, I deem it interesting to summarize the journey to obtain a quantified chemical composition at nano-scale starting from an EELS spectrum. In most of the current microscopes, the different

routines are partly scripted which greatly facilitates the operation. However, the reliability of the results and their accuracy are still heavily user-dependent.

The quality of quantification already starts with requirements to obtain a valuable dataset: the sample preparation, and the microscope setup (CCD camera setup, microscope alignment and illumination setup, choice of acquisition parameters to balance acquisition time / signal-to-noise ratio / sample damages / hardware limitations, determination of the convergence and collection semi-angle ($\alpha$, $\beta$)). Then one still needs to process the data to extract the valuable information.

To do so, the following steps are followed:

- Camera gain reference and dark reference correction
  This has to be done to remove contribution of the camera from the recorded signal.
- Signal deconvolution:
  Using the low-loss spectrum via Fourier-Log or Fourier-ratio methods to remove the multiple scattering events. The low-loss may have to employ the same dispersion as the spectrum to be treated.
- Energy window positioning around the elements of interest ($\Delta$)
  Energy range should be large enough to limit the ELNES interference (e.g. 30 – 50 eV)
- Background correction of the spectrum
  Usually based on a power law approximation, the background correction is one of the most user sensitive parameter.
- Edge intensities measurement over $\Delta$
  Automatically done from the energy ranges defined earlier
- Computation of the partial cross-sections $\sigma$ of the different elements ($\alpha$, $\beta$, $\Delta$, $E_0$)
  Digital Micrograph's script follows the theory outlined in Egerton's work. The calculation requires to know ($\alpha$, $\beta$) semi-angles for the acquisition setting used.

Then, a relative quantification is obtained using the relation:

$$N_a/N_b = \sigma_b/\sigma_a \times I_a/I_b$$

with N the number of atom per unit area, $\sigma$ the partial cross section and I the signal intensity.

### 3.3.3 Sample limitations

**a. Thickness effect**

The sample transparency for EELS measurement is quite important and the optimum thickness can be defined as the compromise between Signal-to-Background Ratio (SBR) and Signal-to-Noise Ratio (SNR). A thick sample will increase the count statistics and lower the noise level, but it will also increase the multiple scattering events and lower the SBR, hence offers a poorer detection level. The relative thickness (t/λ), where t is the sample thickness and λ the fast electron wavelength, seems to be optimal from approximately 0.15 to 0.4. (cf. Figure 18). Additionally, as shown in Figure 19, strong thickness variation of the lamella can directly affect the EELS signal intensity.

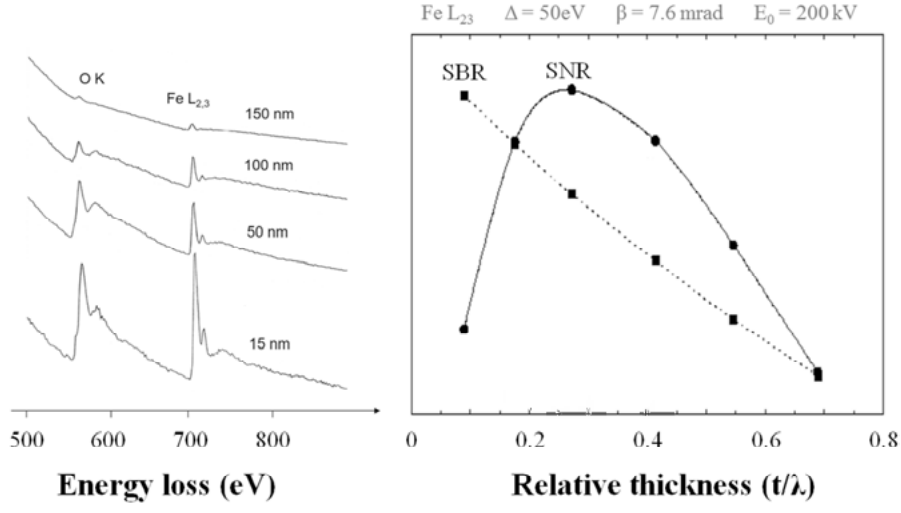


Figure 18 Thickness effect on the Signal-to-background ratio, and optimal relative thickness to maximize the signal-to-noise ratio. Reproduced from G. Kothleitner, PhD Thesis, Graz University of Technology (1996), Austria

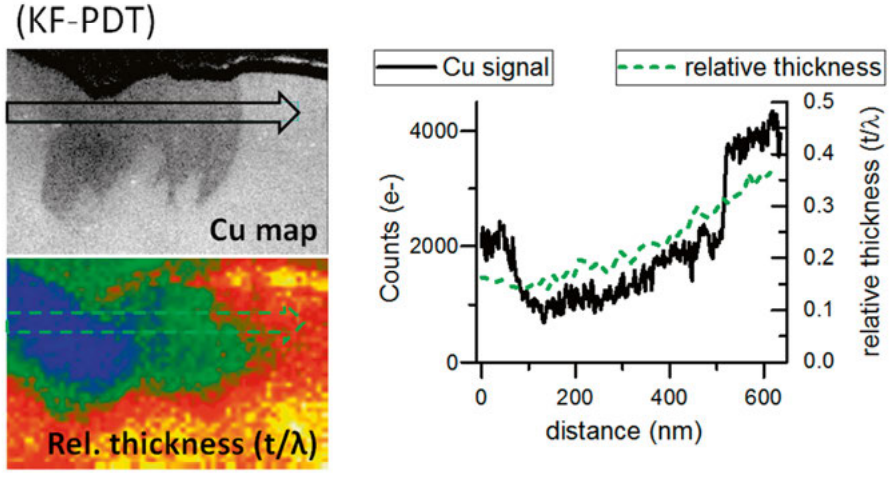


Figure 19 Thickness dependence of the EELS signal reproduced from **Paper IV**. This illustrates the direct dependence of the signal intensity with the lamella thickness. It also shows that once the varying thickness effect is corrected, the Cu content within the patch is rather constant (and different from the concentrations on either side of the patch).

### b. Beam sensitivity

While adjusting the acquisition settings to obtain higher data quality with a minimum amount of noise, we may wish to crank the beam current density up or to extend the acquisition time. However, the sample may not appreciate this intensive nor extended shower and can be damaged. The scanned area may look funny after a mapping which of course questions the validity of the measured dataset and should be considered as an invitation for the operator to repeat the acquisition on a fresh area using milder settings. Figure 20 shows the contrasts generated in a CdS buffer layer after the completion of a single EELS map.

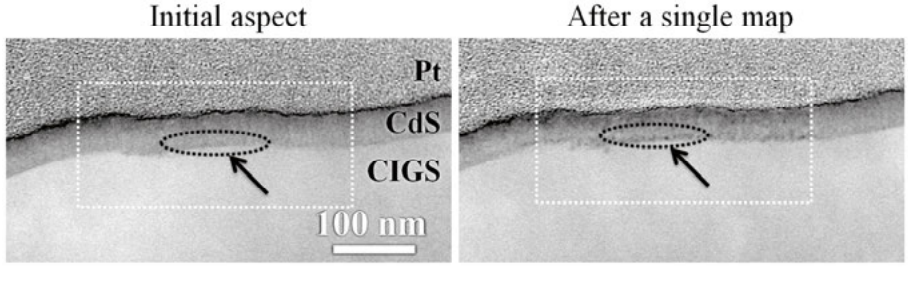


Figure 20 STEM mapping damages of the CdS buffer layer after one acquisition. The white dashed rectangle delimits the scanned area. Many areas with dark contrasts are generated during the electron beam exposure as exemplified by the broken ellipse.

In Figure 21 below is an example of electron-beam induced changes. The changes occurred while I performed a high-resolution observation of a (Zn, Sn)$O_x$ buffer layer deposited by ALD. The originally nearly amorphous layer was completely changed, featuring signs of crystallization after a few minutes of electron beam exposure. The beam-induced mobility of the different chemical elements is then to be questioned when trying to analyze sub-nanometer events.

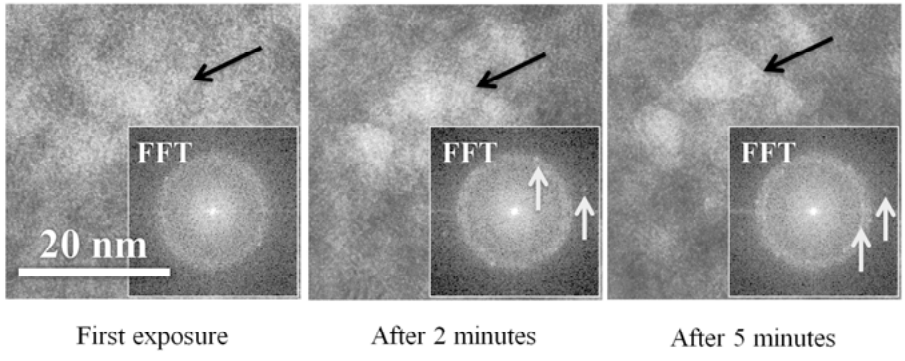


Figure 21 Electron-beam induced crystallization. High-resolution (HR) observation over time of a (Zn,Sn)$O_x$ buffer layer deposited by ALD. The black arrows point to the same spot over time. The Fast Fourier Transform (FFT) of the HR images feature increasing number of spots which confirms the crystallization of the layer.

### c. TEM quantification: Human factor

Repeatedly using the same technique - and being human - may bring overconfidence in equations and lead to the belief that this technique is more precise than what it actually can be. EELS quantification is unfortunately user dependent and the following sentence from R. Egerton's book is self-explanatory *"the success of basic operations such as the subtraction of instrumental and pre-edge backgrounds still depends on the skill of the operator[...]"* [62]. I would rephrase this as: "the precision of the technique may be better on a Tuesday morning than on a Friday afternoon". The usual 10% uncertainty sounds reasonable, nonetheless, my experience also reveals that this number can change from one dataset to another. Indeed, if one cumulates noisy data (to limit the sample damages) with possible ghosting of the CCD (from previous measurement of the intense Zero-loss peak (ZLP) or correction of the intense electron Ronchigram [k]) then the quantification becomes quite sensitive to the background correction and the energy window positioning. This explains why, in **Paper IV**, I employed the trustworthy XRF results as a reference for the EELS quantification output.

[k] The electron Ronchigram is an image of the sample acquired with a fully focused probe that allows correcting the probe's astigmatism and coma aberrations.

## 3.4 Energy-Dispersive X-ray Spectroscopy (EDS)

### 3.4.1 Principle

Energy Dispersive X-ray Spectroscopy (EDS) is a well-spread technique to perform chemical mapping and is directly related to EELS from a physics point of view. In EDS, we observe the X-rays released during the relaxation of the excited atoms of the sample, when electrons transit from higher electron shells down to the lower ones. These X-rays follow then approximately the characteristic inter-shell transition energies, as only minor losses may occur.

It is interesting to specify that X-ray and Auger emissions are two competing phenomena, and the ratio of the two is designated as the fluorescence yield. As a rule of thumb, we would remember that lower atomic numbers display lower fluorescence yield, explaining the challenge of measuring lighter elements by collecting X-rays [60] (cf. Figure 22)

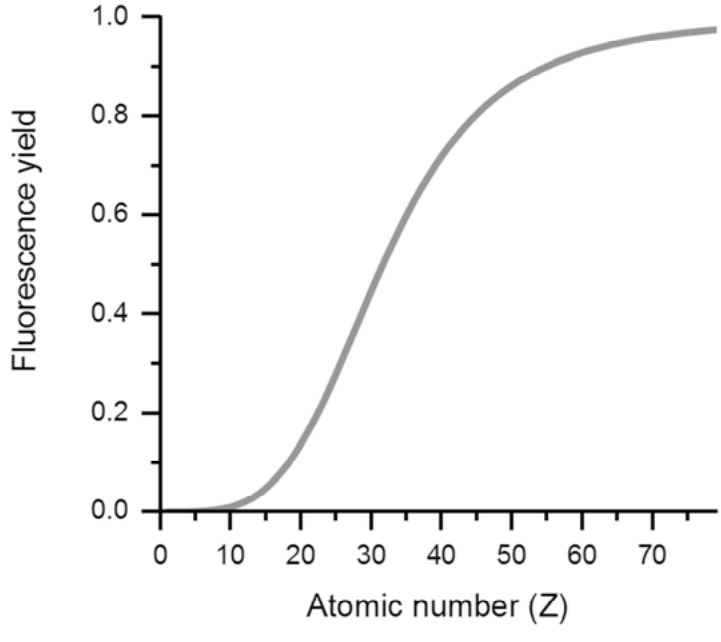


Figure 22 X-rays/Auger fluorescence yield described with a $Z^4/(10^6+Z^4)$ function. The lower X-ray yield for the lighter elements makes their detection harder with EDS techniques.

### 3.4.2 Quantification

The use of a transparent lamella decreases the absorption and fluorescence X-rays and globally lowers the background level. This allows the use of the thin-foil criterion, simplifying the quantification process [64].

Concerning the data acquisition, the sample should be orientated in the holder to have the thin part of it facing directly to the detector, which greatly limits the X-rays absorption. In addition, the illumination settings should be adjusted to maximize the count rates in respect to the detector limit and the beam sensitivity of the sample.

Data processing:

- Background subtraction
  Always double-check that the background windows are not placed over X-ray peaks (scripts still miss a brain)
- Peak intensity integrations
  It is necessary to control the residual background to verify the quality of the peak fitting.
- Determination of the k-factors
  They depend on the acquisition conditions and detector configuration
- Using the thin foil criterion assumption, the elemental concentrations are calculated using the following Cliff-Lorimer equation:

$$C_a/C_b = k_{ab} \times I_a/I_b$$

with C the atomic concentration, k the k-factor and I the signal intensity.

## 3.5 Electron diffraction

The electron diffraction analysis is actually complementary to X-ray diffraction. Indeed, the electron-matter interactions, originating from coulombic interactions with atoms of the sample, are much stronger than the X-ray-matter ones. Therefore, when a sample is said to be “X-ray amorphous”, electron diffraction can probe its structure down to the nanometer scale and sometimes reveals the presence of nano-crystals.

For both techniques, coherent waves are sent to the sample. The periodic structures of the crystal scatter them and, at specific angles, form constructive wave interferences (cf. Figure 23). The diffraction angles are recorded, and using the Bragg’s law, the real lattice inter-planar spacing can be calculated using the equation:

$$n\lambda = 2d_{hkl}\sin\theta$$

with λ the electron wavelength, $d_{hkl}$ the inter-planar distance, and θ the diffraction angle fulfilling the Bragg condition [65].

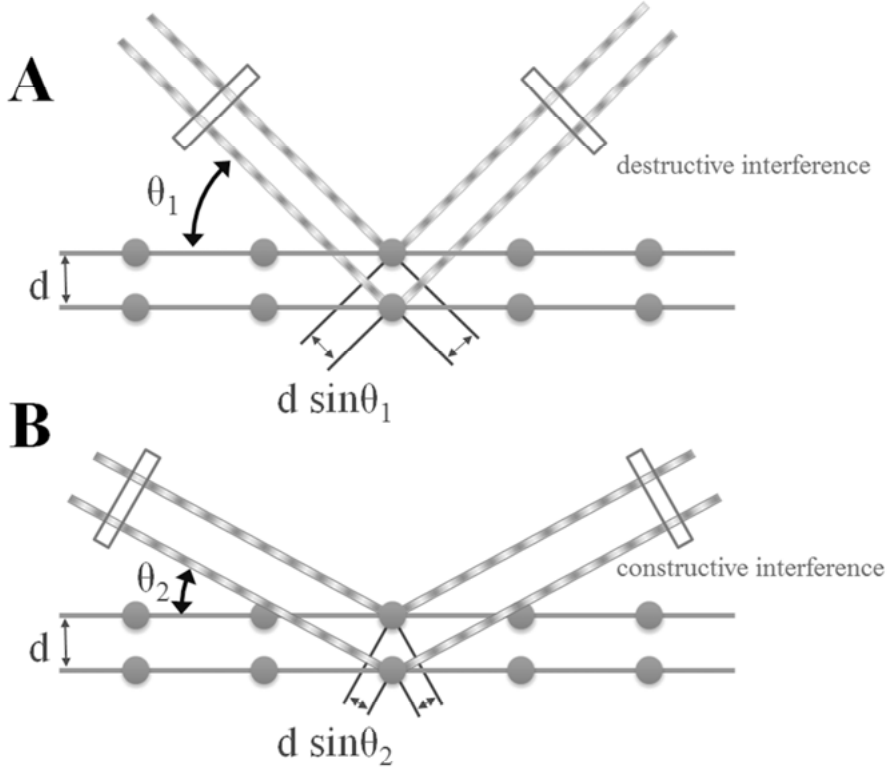


Figure 23 Sketch illustrating the Bragg condition. The path difference between two parallel waves depends on the incident angle (θ) and the lattice spacing (d). At random angles, the path difference between the two waves results in non-constructive interferences (A). The Bragg condition is fulfilled when the path difference is a multiple of the wavelength (nλ), with n being an integer, allowing a constructive interference between the diffracted waves (B).

In reciprocal space, the incident wave can be described by a vector $\mathbf{k_0}$, with $||\mathbf{k_0}|| = 1/\lambda$. As we only consider elastic scattering, the diffracted wave can be described by a vector $\mathbf{k_s}$ of the same length as $\mathbf{k_0}$ but of a different direction. Doing so, we build the Ewald sphere where the Bragg condition is satisfied when the vector $\mathbf{k_s} - \mathbf{k_0} = \mathbf{g_{hkl}}$ lies at the surface of the sphere as illustrated in Figure 24.

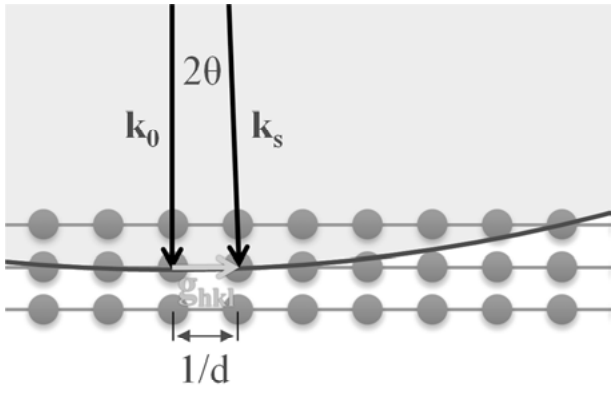


Figure 24 Sketch of the Ewald sphere construction of radius 1/λ. The Bragg condition is verified for the atoms crossing the outersphere, meaning $\mathbf{g_{hkl}} = n \times 1/d$ corresponding to $n \times 1/d = 2 * 1/\lambda * \sin\theta \Leftrightarrow n\lambda = 2\, d \sin\theta$ (i.e. the Bragg's law)

*Diffraction analysis:*

The analysis begins with the orientation of the crystal. To do so, I have used the Kikuchi pattern which rapidly allows identifying the principal zone axes (ZA). As each DP gives only planar information, I have acquired several diffractograms from multiple directions to recover the 3-dimensional information [64]. This was used for the secondary phase analyses in **Paper IV** and **Paper V**. The DP analysis was performed using JEMS and CrysTBox [66] correlating the tilt angles and the potential ZA angles to identify the correct space group. When possible, the results were completed with XRD measurements.

## 3.6 XRD, XPF, PL and other wild acronyms

Here is a *very* brief summary of the techniques encountered during this thesis.

### a. X-ray Diffraction (XRD)

*Uses:*

Crystal structure and phase determination.

*Principle:*

Monochromatic X-rays (e.g. Cu $K_\alpha$) are directed to the sample surface and the crystalline part of it generates a diffraction pattern. The position of the spots in the diffractograms can be related to the crystal lattice parameters as described by the Bragg's law. The intensity of the spots can provide further information concerning the texture or the fraction of the present phases.

**b. X-ray Fluorescence (XRF)**

*Uses:*
Analysis of the chemical composition.

*Principle:*
Characteristic X-rays are directed onto the sample surface to trigger ionization events of its atoms. While the exited atoms of the sample relax to their initial state, they can generate secondary X-rays characteristic of the sample constituents. Therefore, monitoring the secondary X-ray emission will allow identifying the elements present in the sample.

**c. X-ray Photoelectron Spectroscopy (XPS)**

*Uses:*
Identify chemical bonds at the very surface of a sample

*Principle:*
The measured sample is exposed to monochromatic X-rays of a defined energy which induces emission of photoelectrons. By measuring the kinetic energy of these photoelectrons, one can calculate the original electron binding energy thanks to the known excitation source. And because the electron binding energies depend on the chemical binding state, it is an elegant way to assess the state of the surface chemistry. Finally, the photoelectron energy being low they hardly escape the bulk, hence the results usually originate from within the first nanometers from the surface.

**d. Photoluminescence spectroscopy (PL)**

*Uses:*
Information about the electronic structure (e.g. the band gap)

*Principle:*
We will restrain the description of the technique to its use in the present work.

A light source of energy larger than the band gap (e.g. laser 785 nm) is directed onto the sample and generates electronic transitions by photo-excitation. After a short time-lapse (the carrier lifetime) the electron-hole pairs created recombine through either radiative or non-radiative processes. The wavelength and intensity of the emitted light provides valuable measurement of the band-gap value and a qualitative measure of the radiative/non-radiative recombination processes, respectively.

### e. Raman Spectroscopy (named after the physicist Sir C. V. Raman)

*Uses:*
Identify specific crystal phases

*Principle:*
A monochromatic light (e.g. laser) illuminates the surface of the sample. A fraction of this light triggers phonons which are characteristic vibrational modes of crystal phases. This process being inelastic, the illuminating light transfers a portion of its own energy to the crystal lattices. By measuring the energy spread of the reflected light, one can display the vibrational modes of the sample lattices and link it to the presence of certain phases. This inelastic energy transfer is referred as the Stokes Raman scattering, and can also occur in the other way around, where the lattice transfers energy to the reflected light. This simply displays in the analysis as pair of peaks.

### f. Electron-Beam Induced Current (EBIC)

*Uses:*
Assess the quality of the charge carrier collection in a semiconductor device

*Principle:*
A semiconductor device (e.g. solar cell) is placed in a SEM and electrically connected to a current amplifier. The electron-beam scans the device which generates electron-hole pairs that can diffuse and drift and induce a current. The measured electro-current is directly related to the carrier collection efficiency. Therefore, with a constant electron beam current and assuming a constant carrier generation rate, a lower current output would indicate a higher charge-carrier recombination or a worse carrier collection (cf. example Figure 25).

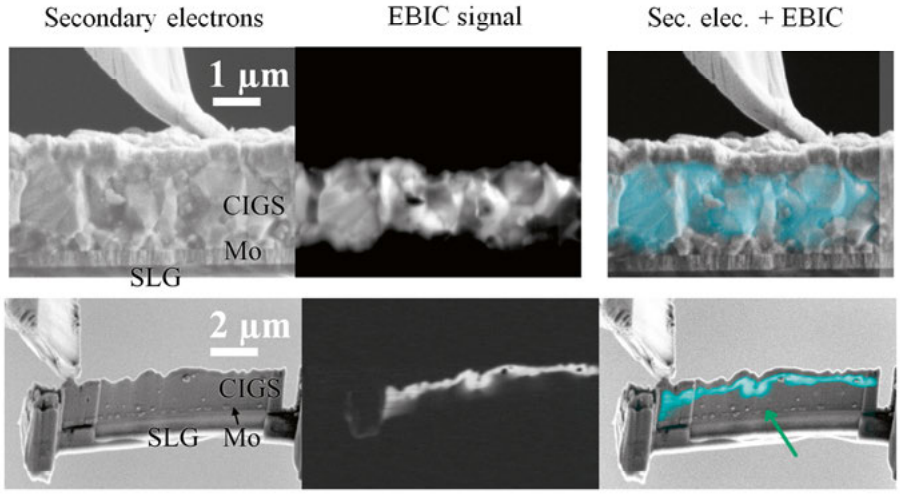


Figure 25 EBIC cross section measurements of the same sample performed at 5kV. Two preparation methods are demonstrated: the CIGS solar cell was freshly cleaved (top) and I extracted a TEM lamella using the FIB in-situ lift out technique and passivated it with a 10 nm-$Al_2O_3$ layer deposited by ALD (bottom).

# 4 Experimental details

## 4.1 Focused-Ion Beam (FIB)

The FIB sample preparation is one technique among numerous others [67] but is extremely attractive. It is favored for being fast, usually 4h start to finish, for allowing a lamella preparation precisely located on the sample, and for being adaptable to most of the materials that we may encounter, from ceramics to living matters [68]. Moreover, it benefits from a high success rate above 90 % [69], which spares a significant amount of time (and frustration) dedicated to the sample preparation. Overall, this preparation technique leads repeatedly to a high-lamella quality with a reasonable training period, which is marvelous for accurate and consistent TEM analyses. The main-stream preparation techniques are based on the "in situ lift-out" as developed by Langford and updated since then [69–72].

On the downside, the price and running cost of such a tool is far from affordable, and if the list of users extends too much, it might delay the sample preparation. And as for any preparation techniques, this one can induce its own preparation artifacts as described in the following.

### 4.1.1 Principle

The FIB is actually a scanning electron microscope (SEM) equipped with an additional ion beam as pictured in Figure 26. Similar to electrons, ions are charged particles and can be controlled by the means of electrostatic Einzel lenses allowing for focusing them precisely in a spot. The ions are typically accelerated between a few hundreds of volts and 30 kV, which grant them enough kinetic energy to sputter the atoms off a target. Thus, the ion beam can be utilized to etch and polish a thin lamella out of a bulk sample. The ion-beam is generally Ga-based (gallium liquid metal ion sources (LMIS)), but alternative gas field ionization sources (GFIS) have been recently introduced [73].

The FIB is also equipped with additional gas nozzles located close to the surface of the sample. They allow for injecting different useful chemical components, some to enhance the etching rate (e.g. $H_2O$, $XeF_2$) and other to deposit material (e.g. Pt or SiO2 precursors). The in-situ material deposition is a beam-assisted deposition and not a simple condensation (at room temperature! Cryo-preparation is another topic). In this way, the deposition rate

is the highest directly under the electron beam (or ion beam) and can be accurately controlled down to the sub-micrometer range.

The ion-column and electron-column are positioned with a fixed angle in between (e.g. 52˚ in the FEI Strata DB 232). So when the ion beam is working perpendicularly to the surface of the sample, the electron beam can be used to observe the cut (or build) from the side. It is extremely useful to observe and control the depth of the cuts and the polishing progress of a TEM lamella.

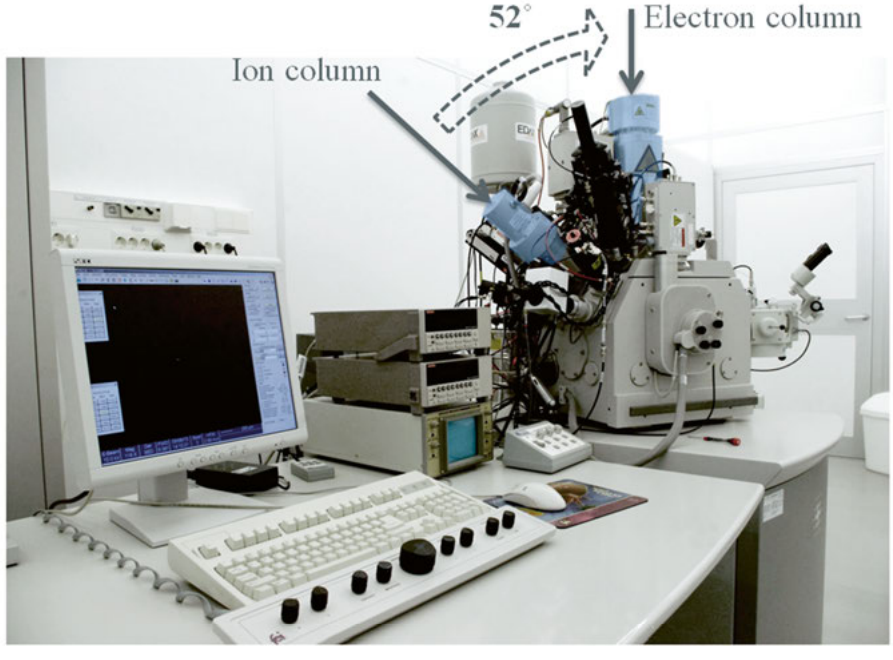


Figure 26 Picture of the Focused ion beam (FIB) Strata DB 232 from FEI that I used during this thesis. The electron and ion columns (highlighted in blue) are squeezed between the nano-manipulator, the different detectors and the multiple gas nozzles.

### 4.1.2 Ion beam damages

When ions collide with the surface of the sample, a portion of them penetrates into it and damages the crystal structure [74,75]. However the depth of such damages can be greatly minimized by the use of a lower accelerating voltage [76,77]. The stopping and range of ions in matter (SRIM) simulation, as shown in Figure 27, is a great tool to estimate this penetration depth [78].

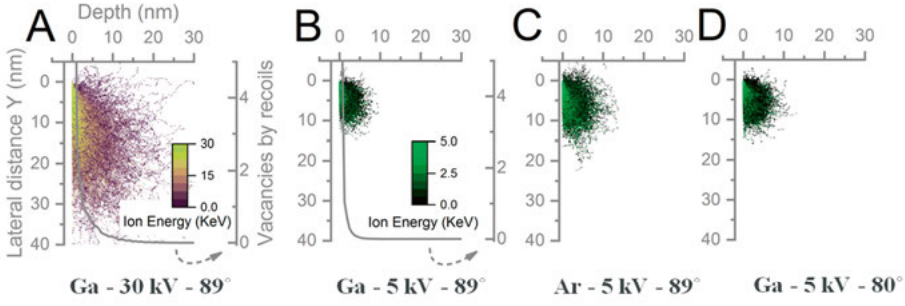


Figure 27 Stopping Range of Ions in Matter (SRIM) simulation. The result shows the penetration of ions in CIGS as function of the ion type, the incident angle and the accelerating voltage. We observe that the ion acceleration voltage is the predominant factor for the penetration depth.

While travelling into the sample, ions may bounce outwards again or stay implanted, changing artificially the local chemistry [79]. Finally, possible re-deposition phenomena and phase separation may be observed [80].

A side-effect of the ion bombardment is the accompanying heat-transfer. Although such a phenomenon is a hassle to measure, several reports evaluate that the temperature of the lamella can rise from tens to several hundreds of degrees, enhancing chemical reaction, diffusion and evaporation phenomena [81–83].

From these, it is clear that the lamella observed in the TEM can be different from the original bulk sample that we want to analyze [84]. My answer to this problem was to correlate different measurement techniques as for instance in **paper V**.

## 4.2 FIB sample preparation for TEM analysis

### 4.2.1 High quality, reproducible preparation baseline

The following TEM lamella preparation is my baseline developed during this thesis, based on the in situ lift-out technique as mentioned in the theoretical part.

The area of interest is first identified and protected with Pt. The Pt deposition is achieved by electron-beam assisted deposition using 2 keV beam energy, a 2000-µm wide aperture and the highest spot size (7). The low beam energy yields a higher cross section with the gas precursor, and the extreme aperture and spot size offer a very high beam current, hence a much faster deposition rate. I approximately set the deposition area to 4 x 20 µm, the duration to 5 min which gives a 2 µm-thick Pt protective cover. I favored

the electron deposition over the ion deposition because of the lower risk of damaging the surface to observe, and also because it results in finer Pt grain structures which reduces the curtaining effect later in the polishing [71].

The first cut-out prior to the lift-out is controlled by script in order to always obtain the exact same lamellae to start with the polishing step. The script uses a 30 kV Ga-based ion beam but I modified it to regularly decrease the beam currents from 5000 pA to 300 pA when approaching the final definition of the rough lamella (final dimensions are 15 µm long, 1.5 µm thick, 5 µm deep). I manually cut free the lamella and lifted it out using a nano-manipulator (Omniprobe from Oxford instruments). Finally, the lamella is attached to a Molybdenum grid using a Pt soldering on both faces for an increased thermal conductivity and stability.

The polishing is manually performed as follow:

- 30 kV 300 pA ± 1° down to 500 nm in thickness
- 30 kV 100 pA ± 1° down to 300 nm in thickness
- 30 kV 50 pA ± 0.6° down to 100 nm in thickness (with $XeF_2$)
- 5 kV 50 pA ± 10° down to approximately 50 nm (with $XeF_2$)

We note the decreasing acceleration voltage and beam current to limit the ion penetration depth and heat amount transferred to the sample. The thickness as viewed from the top is extremely hard to estimate from below 300 nm, especially if we consider both the slight lamella tilt, the possible bending, and the poor resolution obtained with lower accelerating voltages in our system. To estimate the thickness, I extensively used the electron beam and the changing electron transparency of the lamella. In fact, when the thickness is low enough, the fast electrons from the beam begin to reach the opposite side of the lamella, and generate additional secondary electrons there leading to a much brighter signal collected. I successively decreased the electron beam energy from 10 keV, to 5 keV and finally to 3 keV which leads to a transparency effect when the sample is thinner than approximately 300 nm, 100 nm and 50 nm, respectively [85] (cf. Figure 28). The transparency is not exactly an ON/OFF state but is fairly easy to apprehend as pictured in Figure 29. One should be aware though that in a second phase, the sample thickness starts to limit the cross section for an electron to interact with the sample, making the recorded signal darker again (soon to become a hole!). This method, given that we repeatedly prepare similar samples, turns out to be quite reliable.

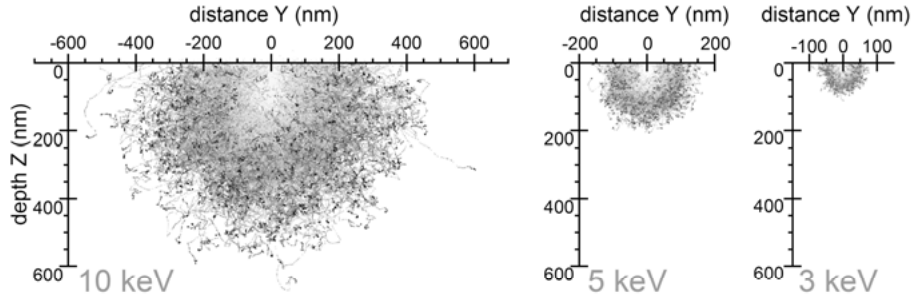


Figure 28 Monte-Carlo simulation that I used to estimate the electron transparency of the CIGS lamella depending on the fast electron energy (CASINO simulation v2.48) [85]

I performed the ion polishing at 30 kV accelerating voltage using a "cleaning cross-section" pattern (ion beam focused on one line gradually moving forward), but the 5 kV polishing using a rectangle pattern (in which the beam is continuously swept). The deteriorated resolution observed using low accelerating voltages together with the possible lamellae deformation generally prevent the use of the same "cleaning cross-section" pattern for the last polishing. This poor capability of focusing the ion beam accurately with voltage below 30 kV also explains why I excluded the use of intermediate voltages during the polishing steps; they mostly erase the protective Pt cover.

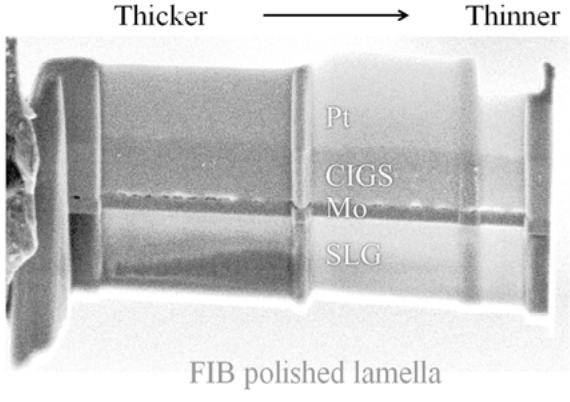


Figure 29 Apparent electron transparency of a TEM lamella as viewed during the FIB polishing. Electron beam energy is set to 5 keV.

### 4.2.2 Preparation artifacts

The polishing step may be tedious and can be overlooked. However, qualitative and reliable TEM measurements are only possible if the preparation is well controlled.

My preparation baseline has been elaborated in order to limit the presence of the most common artifacts. The final polishing step with low energy Ga-ions removes most of the crystal structure damages from the higher energy steps (cf. Figure 27). The curtaining effect, affecting the thickness homogeneity of the lamella, was improved by using electron-deposited Pt and by removing the surface precipitates. In my experience, the precipitate formation seems to be independent of the ion beam energy and current, but is enhanced by electron-beam exposure as shown in Figure 30, so I kept the electron observations as few as possible. The implementation of $XeF_2$ as reported in the literature seems to be the only viable solution to erase them efficiently [72,86].

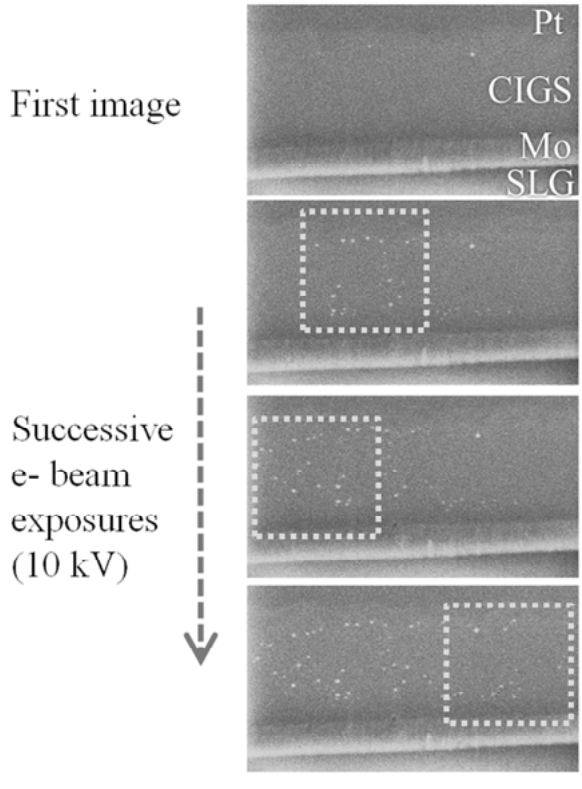


Figure 30 Surface precipitates growth under e- beam exposure; the dotted squares symbolize the area scanned with e- beam before the image was recorded.

From **paper IV**, the repeated FIB preparation and TEM analysis of the same samples eventually allowed me to identify an important preparation artifact that was not yet reported, or not linked to the sample preparation [87]. The chemical composition maps revealed important amount of $Cu_{Cd}$ substitution, where none or only seldom inclusions have been previously reported [88–90]. Performing dedicated observations of the same lamella polished in two sequences, I could confirm that it was induced by the FIB sample preparation.

This phenomenon was increased when the switch to lower ion beam energy was delayed (i.e. the lamella thickness was thinner than targeted). $Cu_{Cd}$ substitution is a gradual phenomenon starting at the interfaces of the buffer layer and can lead to an almost complete modification of the buffer layer as shown in Figure 31.

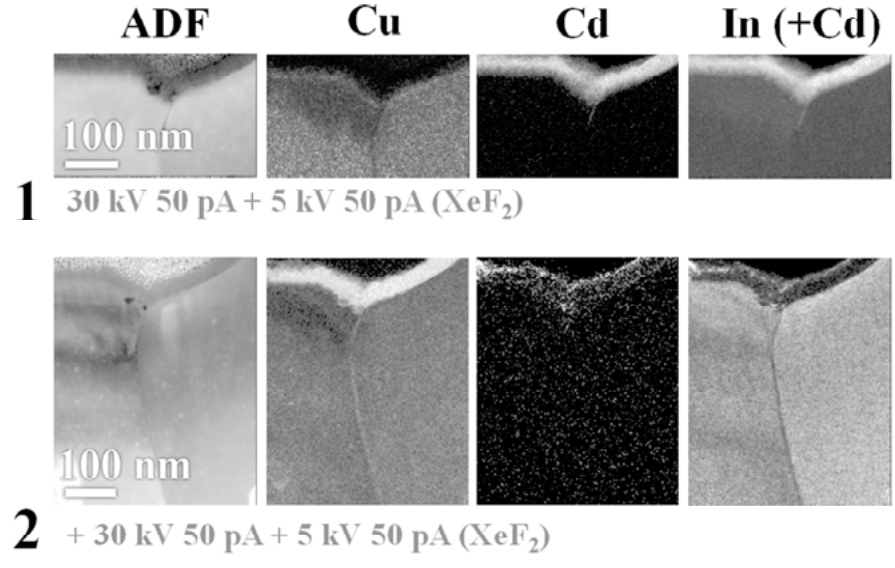


Figure 31 FIB-induced $Cu_{Cd}$ substitution. Same sample, same area observed once (1) and repolished prior to a second observation (2). After the second polishing, most of the Cd is gone and replaced by Cu, but the other CIGS elements seem to behave and stay in the absorber layer. Note that the Cu-content of the grain boundary also changes from low to high after the second polishing.

### 4.2.3 EBIC targeted preparation

Though targeted sample preparations are quite accessible using a FIB, it is slightly more complex when the target is several microns below the surface of the sample. For **paper III**, the goal was to analyze the rear-passivation layer openings in their center. The diameter of the openings and their spacing was to be measured; therefore, I could not take a random cut as a first choice. Instead, I acquired an EBIC signal to locate the opening rows. Correlating small surface features between the secondary electron image and the EBIC one, and thanks to the low amount of drift, I could mark the correct TEM lamella position using the Pt deposition and I then could proceed to the standard preparation. To help my success rate, I added a slight rotation of a couple of degrees between the opening rows and the Pt deposition line. Therefore, out of the five openings contained in one lamella, I could afford to miss a pair of them during the polishing, to have the remaining ones precisely in their center (cf. Figure 32).

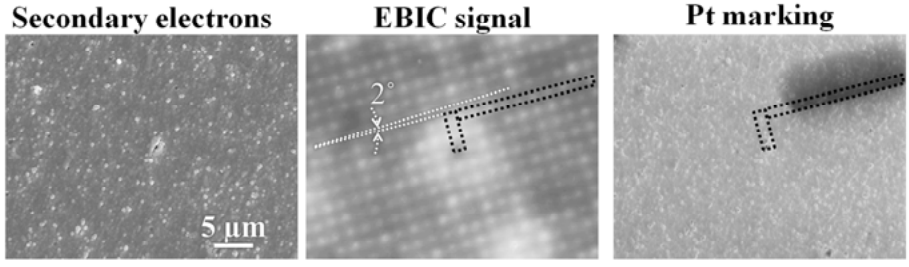


Figure 32 Example of a EBIC targeted preparation using a Pt marking to start the TEM lamella preparation. The secondary electron image shows the surface of the sample. The EBIC signal reveals the opening positions in the passivation layer below the surface and the protective Pt is used as a marker to extract the TEM lamella from the right area.

## 4.3 Solar cell deposition

### 4.3.1 CIGS baseline

The CIGS baseline is our standard cell manufacturing procedure that should ensure a repeatable solar cell quality and performance. I will restrict the process description to the part relevant for this thesis work.

*Cleaning*

All glass substrates are cleaned prior to the back contact deposition. The cleaning is performed using a solution of Cole-Parmer Micro-90 detergent at 60˚C followed by thorough rinsing steps with deionized water.

*Mo back contact*

Two layers of molybdenum, high-pressure / low-pressure, are deposited in one run with our inline MRC 603 system based on DC-magnetron sputtering. The first high-pressure layer only ensures a good adhesion to the substrate and represents approximately 20 nm. The subsequent low-pressure Mo layer is added to improve the conductance of the back contact. The total stack measures about 350 nm in thickness and displays a sheet resistance of about 0.7 Ω/□.

*CIGS co-evaporation*

A 15 nm-thick NaF precursor layer is thermally evaporated on the Mo back contact prior to starting the co-evaporation to ensure a satisfying Na supply to the absorber layer. The precursor thickness is manually monitored using a calibrated quartz-crystal. Then, the CIGS absorber layer is co-evaporated in a high-vacuum Balzers BAK 550 tool. The system uses individual sources placed at the bottom of the chamber: open-boats for Ag, Cu, In and Ga, one

Knudsen evaporation cell for Se and one for the alkali-metals (alkali-metal post-deposition treatment (PDT) is further described in section 4.3.3). Except for the Se and alkali-metal sources, the evaporation rates are power-controlled, but monitored and regulated through a mass-spectrometer feedback system.

The targeted composition for the absorbers is usually Cu/III = 0.9 and Ga/III = 0.4, but can be made flat-profile or Ga/III graded depending on the research. The graded profile follows a Cu-poor, Cu-rich, Cu-poor sequence as shown in Figure 33.

The chemical composition of the completed absorber layers is routinely controlled by XRF analysis to measure the average Ag/I (for ACIGS), (Ag)Cu/III and Ga/III ratios.

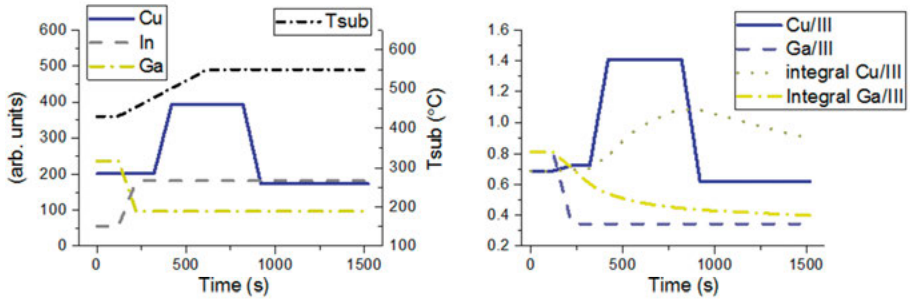


Figure 33 Detailed co-evaporation profile of the CIGS layer, showing the substrate temperatures plotted together with the individual flux variation of Cu, In and Ga (left); and the estimated Cu/III and Ga/III ratios, both instantaneous and integrated (right). The Se source was kept constant during the co-evaporation to ensure a good saturation level. Reproduced from **Paper IV**.

*CdS buffer layer*

The time lapse between the previous vacuum process and this CBD step is kept as short as possible (< 5 min) to limit the absorber degradation as shown in **Paper I**. The cadmium sulfide buffer layers are fabricated by chemical bath deposition (CBD).

If an alkali-metal PDT has been performed, we first pre-heat (to 60°C) a 125 mL solution of ammonia (NH3, 1.7 M) and cadmium acetate (CdAc, 4.5 mM). Then a 50 mL solution of Thiourea (0.35 M) is added to the hot mix and the samples are immersed immediately. The beaker is placed in a water bath at 60°C for 4 min which leads to a 30 nm thick CdS layer.

If no PDT has been performed, the solutions are mixed at room temperature and the samples are immersed directly. The beaker is immediately placed in a water bath at 60°C for 8 min which leads to a 50 nm thick CdS layer.

*The front contact*

The Transparent Conductive Oxide (TCO) consists of two layers. The deposition starts with a 80 nm-thick non-doped ZnO layer (i-ZnO) to limit the possible shunt paths and protect the CdS layer from subsequent damages [91–93], and is followed by a 300 nm-thick aluminum-doped ZnO layer (ZnO:Al). The complete stack displays a sheet resistance of about 40 Ω/□. The layers are deposited by RF magnetron-sputtering using a Von Ardenne CS600S system.

The Ni/Al/Ni metallic contact stack (60 nm / 2 µm / 60 nm, respectively) is then deposited using electron beam evaporation through a shadow mask. Finally, the individual 0.5 $cm^2$ solar cells devices are electrically separated by mechanical scribing. The completed cells are pictured in Figure 34.

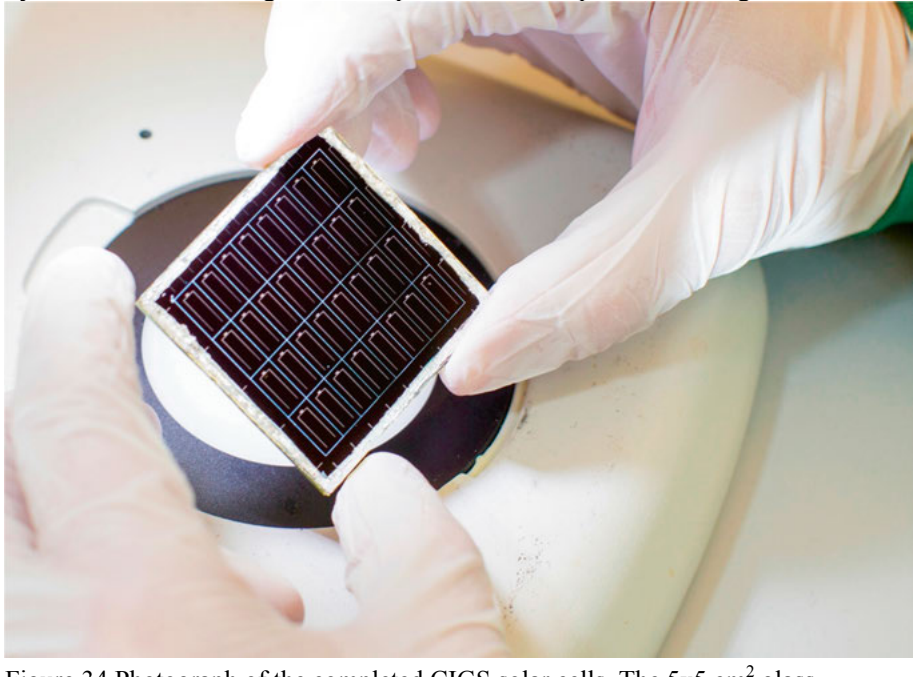

Figure 34 Photograph of the completed CIGS solar cells. The 5x5 $cm^2$ glass substrate contains 32 individual devices (4 x 8), each with an area of 0.5 $cm^2$.

### 4.3.2 Atomic layer deposition (ALD)

The ALD is a vacuum based process that can be used to deposit both alternative buffer layers (e.g. ZnSnO or Zn(O,S)) and passivation layers. The principle of the technique is to fill the chamber with a gaseous precursor, flush it with a neutral gas to remove the excess, fill the chamber with a second gas that will react with the first (adsorbed) precursor and flush it again with a neutral gas. Each of these cycles will add about one monolayer of new material (e.g. 0.9 Å/cycle), and they are repeated until the desired thickness is obtained.

Our $Al_2O_3$ passivation layers were deposited in a Picosun Sunale R200 system using a trimethylaluminum (TMA) precursor and water as co-reactant. The reaction chamber was stabilized at 300°C prior to the beginning of the deposition. Typical passivation layer thicknesses range from 1 to 30 nm.

When set below the CIGS absorber layer, the passivation layer prevents the out-diffusion of sodium from the SLG which requires a subsequent supply of Na to maintain the cell electrical performance.

### 4.3.3 Alkali-metal Post-Deposition Treatment (PDT)

This operation is performed in the Balzers BAK 550 system using the dedicated Knudsen evaporation cell as described in section 4.3.1. The evaporation flux is measured by a dedicated quartz crystal previously calibrated, and adjusted by manually tuning the heating power. The alkali-metal-PDT is performed in-situ immediately after the absorber layer deposition. The chamber stays under vacuum all the time but the substrate temperature is lowered and stabilized at 350°C before starting the treatment. While the samples are shielded with a physical shutter, the alkali-source is heated up and stabilized to obtain a deposition flux of approximately 5 Å/min. Then the shutter is opened for 10 min and closed again. A low Se pressure is maintained during this operation. Finally, the temperature control for the substrates and the sources is turned off, and the system naturally cools down in vacuum before the chamber is vented and opened. The substrate temperature is normally at about 100°C, when the chamber is vented.

# 5 Overview of the appended papers

Electron microscopy is an eye for the scientists. When surface sensitive techniques such as X-Ray Photon Spectroscopy (XPS), Raman or even Glow Discharge Optical Emission Spectroscopy (GDOES) can detect subtle chemical contributions, they suffer from limited spatial resolution which only allows averaged measurement values across the surface. This is where Electron microscopy is a game changer. It is usually less sensitive detection-level-wise, but its spatial resolution and ability to analyze deep cross-sections allow studying the local aspect of a phenomenon at the nanometer scale, even several micrometers below the surface. And as each technique has assets, it seems natural to correlate them in order to perform both sensitive and spatially resolved measurements.

In the following, a collection of the work produced during this thesis is presented. The order is rearranged thematically to ease the reading and may differ from the actual chronology.

## 5.1 Rear interface: Papers I, II, III & VI

### 5.1.1 Paper II - Surface defect passivation by a thin metallic barrier for $Cu(In_xGa_{1-x})Se_2$ co-evaporation on Cr-steel substrates

*Background*

When reading literature concerning the use of steel as a CIGS solar cell substrate, two conclusions stand out: with no additional barrier the cell efficiency is dramatically reduced due to detrimental out-diffusion of ions from the steel substrate (c.f. section 2.7.1), and only thick barrier layers seem to lead to equal performance to those obtained with a SLG substrate. The barrier thicknesses range from hundreds of nanometers for pure Cr, up to several micrometers for oxide layers. While steel roughness has been regularly mentioned as a problem [94–96], using polished substrates did not always lead to good working cells. This study had the ambition to analyze the exact ion leakage mechanism responsible for the cell contamination, inspecting the pin-hole formation through different thin metallic barrier layers. Electron

microscopy was the ideal tool for such chemical analysis of local defects, explaining its central presence in the article.

*Key findings*

- Local but deep surface imperfections originate from loosen chips of steel encrusted on the surface during the steel rolling process.
- Micrometer-deep gaps around them induce discontinuities in thin-sputtered barriers.
- Peak-to-valley roughness value, describing more accurately the local surface topography, should supplement the common average roughness value to characterize sample surface quality
- Cr-metallic barrier reacts with Se, lowering direct exposure of the steel surface to it. This chemical barrier limits the massive out-diffusion of detrimental substrate components that was observed with a Ti-metallic barrier.

*Personal contributions*

Almost all of the writing, sample processing, FIB sample preparation, TEM EDS analysis and most of the interpretation

### 5.1.2 Paper I: On the assessment of CIGS surface passivation by photoluminescence

*Background*

When trying to reduce the thickness of the absorber layer, the high interfacial recombination rate drastically reduces the output efficiency of the device [56]. This study assessed the passivation capabilities of $Al_2O_3$ oxide layer by observing the PL intensity at the rear-interface. To do so, a semi-transparent Mo back contact was employed, offering the advantage of being very similar to our baseline Mo back-contact in terms of interfaces. Charge carrier recombination occurring via defects is essentially non-radiative, therefore, measuring the radiative/non-radiative component was a good indicator of the interface quality. I performed a TEM cross-section analysis to ensure that the integrity of the test structure was conformed to the expectations and preserved after the CIGS co-evaporation.

*Key findings*

- A semi-transparent back-contact representative of the baseline structure has been developed and allowed PL measurements from the rear interface.
- Rear-interface passivation was stable over several weeks.
- PL intensity increase indicates that the rear-surface recombination rate was lowered by addition of an $Al_2O_3$ passivation layer

*Personal contributions*

Electron microscopy experiments planning, execution and interpretation, article discussion and minor part of the writing

### 5.1.3 Paper III: Rear surface optimization of CZTS solar cells by use of a passivation layer with nanosized point openings

*Background*

The passivation benefits were previously confirmed with CIGS absorber layers. This work implemented the passivation in a thin (400 nm) $Cu_2(Zn,Sn)(S,Se)_4$ (CZTS) absorber layer. Current-Voltage (J-V) and External Quantum Efficiency (EQE) measurements confirmed a positive passivation effect, but the peeling-off incidents remained unexplained. We needed to observe what the rear-passivation became once the stack was completed and the TEM was then a well-suited instrument for the task. The goal was to analyze the nano-openings in their center and the state of the remaining passivation layer. For this work I used the EBIC targeted FIB sample preparation as described in the experimental section.

*Key findings*

- $Al_2O_3$ passivation layer was successfully implemented in thin CZTS absorber layer (400 nm)
- The addition of a passivation layer had positive impact on each of the electric parameters
- Higher performance was attributed to both a lower recombination rate at the interface and a limited generation of secondary phases at the rear side of the absorber layer (i.e. field effect and chemical passivations)
- Electron microscopy indicated that the enhanced sticking behavior of the CZTS absorber layer relied on the passivation layer openings acting as anchoring points.

*Personal contributions*

EBIC targeted FIB sample preparation, TEM EDS analysis and result discussion. Minor part of the writing

### 5.1.4 Paper VI: Effect of different Na supply methods on thin $Cu(In,Ga)Se_2$ solar cells with $Al_2O_3$ rear passivation layers

*Background*

The goal with this work was to use a passivation layer without openings, but thin enough for the current to tunnel through. To reach comparable cell performance as compared to previous passivation work despite the absence of openings in the $Al_2O_3$ layer, Na provision needed to be ensured. However, if the water soluble precursor layer is not entirely consumed during the absorber growth, the residue can cause the absorber layer to peel off during the Chemical Bath Deposition (CBD) step. To go around this limitation, NaF Post-Deposition Treatment process was implemented, and the comparison between the two Na incorporation strategies allowed us to answer some remaining questions from earlier work. The hypotheses were that the passivation layer was either chemically or physically affected by the NaF precursor layer deposited onto it. I used the electron microscopy analysis to evaluate the local alteration of the passivation layer, and could explain the measured current flow in some solar cells despite the presence of a several-nm thick $Al_2O_3$ barrier layer deposited by Atomic Layer Deposition (ALD).

*Key findings*

- Passivation layer behavior is directly linked to the NaF supply strategy. Using a NaF precursor layer, the current could flow normally even with a 6 nm thick $Al_2O_3$ passivation layer, whereas with a NaF-PDT, the current was already blocked with a 1 nm thick passivation layer.
- TEM analysis revealed that the NaF precursor deposited on the top of the passivation layer can degrade the layer, creating significant openings through it.
- In all cases, a $GaO_x$ layer was measured on top of the $Al_2O_3$ passivation layers after the CIGS co-evaporation process

*Personal contributions*

TEM sample preparation, EELS analysis and interpretation. Result discussion and part of the writing

## 5.2 Front interface: Papers IV & V

### 5.2.1 Paper IV: Deep surface Cu depletion induced by K in high efficiency Cu(In,Ga)$Se_2$ solar cell absorbers

*Background*

Glass manufacturing may appear surprisingly complex and the properties of the final material depend directly on the composition of the glass. Soda Lime Glass, adopted as reference substrate for CIGS, contains SiO2 (72%), Na2O (14%), K2O (1%), and more or less significant amounts of CaO, MgO, Al2O3, SO3 and Fe2O3. Na, out-diffusing from the substrate during the CIGS co-evaporation is frequently reported to be highly beneficial for the solar cells Voc and efficiency. But the glass transition temperature of such SLG is around 570˚C, limiting the solar cell process temperature. To use a higher process temperature, high strain point glass was introduced, but the Na content was much lower and mostly replaced with K. Supplying Na by the means of a NaF precursor layer, the results were quite positive. GDOES preliminary measurements indicated a clear surface modification of the CIGS absorber layer displaying an abrupt and deep Cu depletion. Based on electron microscopy analysis, I could confirm these preliminary results and further establish the shape and the depth of the depleted patches, alongside with their precise chemical composition. Within this work, I also observed inconsistent $Cu_{Cd}$ substitution in the CdS buffer layer, which I could eventually link to a FIB preparation artifact as explained in the experimental section.

*Key findings*

- Providing K during the CIGS co-evaporation slows down the In/Ga inter-diffusion, resulting in a sharper Ga/(Ga+In) gradient
- Formation of Cu-depleted patches can be observed when combining a Cu poor-rich-poor co-evaporation profile with provision of K during the growth
- Even if K if provided during the CIGS growth, solar cells greatly benefit from an additional KF(or RbF)-Post Deposition Treatment.
- No evidence of Cd in-diffusion to the CIGS layer could be observed
- Presence of Cu in the CdS buffer layer was induced by the FIB sample preparation

*Personal contributions*

Almost all of the writing, FIB sample preparation, TEM analysis and EELS quantification, result interpretation.

### 5.2.2 Paper V: Surface Modification And Secondary Phase Formation From a High Dose KF-Post Deposition Treatment of (Ag,Cu)(In,Ga)Se2 Solar Cell Absorbers

*Background*

Adding silver metal in a solar cell when device prices are dominating many discussions might sound absurd; however, the gain from a lowered melting point or a decreased voltage deficit can be quite valuable as detailed in the introduction section. The preliminary results published from our group reported a positive impact of alkali-metal PDT of ACIGS absorber layers, as commonly observed with non-Ag-alloyed CIGS. However, we also reported a high sensitivity associated to the KF-flux value that could easily lead to no-gain or even decreased cell performances. Therefore, we initiated a comparative study between an optimally treated absorber layer and an excessively treated one by tuning the KF-flux. Whereas the XPS measurements could resolve the complex chemistry changes occurring at the surface of the ACIGS absorber, TEM measurements highlighted that the modifications were not restrained to the surface but also altered the bulk material.

*Key findings*

- As reported for CIGS, a controlled KF-PDT is beneficial for the ACIGS solar cell electrical performance, improving the Voc, FF and efficiency
- A 10 nm-thick (Ag,K)$InSe_2$ (AKIS) layer was found at the surface of the absorber layer by XPS and TEM techniques
- Excessive KF-flux during the PDT leads to thicker AKIS surface layer, formation of secondary phases in the absorber bulk and drastically lower cell performances

*Personal contributions*

Most of the writing, all TEM sample preparation, TEM and SEM measurements and analyses, including the diffraction pattern indexing and EDS quantification.

# 6 Summary and perspectives

Among single junction photovoltaic (PV) solar cells, the thin film type, which I studied in this thesis features among the highest conversion efficiencies (around 23%), the highest energy returned on energy invested (EROI), a large selection of possible substrates and a great potential for industrialization. Although maximizing the efficiency of the solar cells is a major concern in the lab, it is not the only research topic. The thickness reduction of the solar absorber as well as the use of alternative substrates such as steel instead of soda lime glass (SLG) has been studied in this thesis. For this purpose, I have worked on the development of various interlayers and on surface treatments, both aiming at either passivating the interfaces or blocking noxious out-diffusion from the steel substrate; all in order to maintain the same conversion efficiency level as compared to the reference thin film solar cells.

To be more concrete, this work has e.g. highlighted the positive effect of an intermediate $Al_2O_3$ layer used to passivate the interface between the absorber layer and the Mo back contact, but also its deterioration when it is set in direct contact with a precursor of NaF. In addition, I have analyzed the defects typically present in the barrier layers used to block harmful diffusions when using steel substrates. I showed that these defects could act as diffusion paths and I identified that they were initially related to the steel manufacturing process. A third component of my thesis concerned the different incorporation strategies of alkali-metals into the CIGS absorber layer, and their links with both the layer composition changes and the solar cell conversion efficiencies. Finally, I analyzed the importance of KF post-treatment intensity applied to a silver-alloyed CIGS (ACIGS) absorber layer. I was able to conclude that an excessive treatment was quite detrimental to the efficiency of the cell, and correlated with both the presence of secondary phases in the solar absorber and a thicker altered surface layer as compared to reference samples with high efficiency.

In this thesis, the use of electron microscopy was essential for examining the local changes in the different samples. Such changes generally occur at the nanometer scale and usually deep below the surface of the sample, but they can strongly influence the electrical behavior of solar cells. The analysis of the crystallinity combined with that of the chemical composition via the EELS and EDS techniques permitted to improve our understanding of the

samples and to revise our models. Since the electron microscopy techniques usually require a sample preparation, significant efforts have been invested in identifying and controlling potential preparation artifacts, in order to create a qualitative preparation baseline using a FIB. As a result, I was able to show that the Cu of the CIGS layer could artificially diffuse into the CdS layer during the polishing step and modify its composition. In general, I have tried to correlate the results from microscopy analysis with other analysis techniques to improve the confidence level of my conclusions.

Electron microscopy analyses have already revealed valuable pieces of information. Nonetheless, questions regarding the semiconductor internal electric field and the local band gap value before and after the various treatments remain and would deserve further analyses.

*Further perspectives*

Energy is a physical quantity involved in any transformation. All our basic needs require the extraction, shaping, transformation and transport of matter, which justifies the major importance of the energy collection and its conversion. In addition, some of the fossil fuels are reaching their production peak, which means that our generation and the future ones have to face a constriction of the most easily accessible energies. Furthermore, the energy policies also seem to evolve and take an interest in new energy sources.

Therefore, a wide panel of alternative energy conversion systems is being developed. However, they are not all equivalent. To judge the viability of the alternatives, I would include two scientific values in the decision loop: the Energy returned on energy invested (EROI) and the Energy payback time (EPBT), which quantify the energy efficiency of a solution and the speed at which the energy invested can be returned, respectively. However, the associated pollutions with each type of energy and their long-term availability must also be taken into account. Nowadays, the major concerns are the price and the atmospheric emissions, so there is a good chance of observing a growth of nuclear, hydro, wind and solar based systems against the dominant fossil fuels.

Using mainly electron microscopy, I tried to contribute to the understanding and the development of the thin-film solar cells, thus adding my own modest tree to the already existing forest of knowledge.

# 7 Sammanfattning och perspektiv på svenska

Bland alla solceller bestående av endast en pn-övergång har tunnfilmssolceller, den teknik som jag studerat i mitt avhandlingsarbete, bland de högsta verkningsgraderna (cirka 23 %), den högsta energiåterbetalningen räknat på investerad energi (EROI), ett stort utbud av möjliga substrat och en stor potential för industrialisering. Även om maximering av solcellers verkningsgrad är viktig i labbet är det inte det enda forskningsområdet. Reducering av tjockleken av det material som absorberar solljuset (absorbatorn) och användningen av alternativa substrat, såsom stål istället för natrium-kalciumglas (vanligt fönsterglas) har också studerats i denna avhandling. För detta ändamål har jag arbetat med varierande mellanskikt och med ytbehandlingar, båda syftande till att antingen passivera gränsytorna eller blockera skadlig ut-diffusion från stålsubstratet; allt för att bibehålla en hög verkningsgrad, jämförbar med solcellsreferenser som tillverkats på natrium-kalciumglas.

Mer specifikt har detta arbete bland annat belyst den positiva effekt som ett mellanskikt av Al2O3 kan ha för att passivera gränsskiktet mellan absorbatorskiktet och bakkontakten av molybden, men också hur detta Al2O3-skiktet kan brytas ned när det kommer i direktkontakt med en tunn film av natriumfluorid (NaF). Dessutom har jag analyserat de defekter som typiskt finns i barriärskikt som har som uppgift att blockera diffusion av skadliga ämnen från stålsubstrat. Jag har visat att dessa defekter kan verka som diffusionskanaler och jag fann att defekterna ursprungligen uppstod vid ståltillverkningsprocessen. Den tredje delen av min avhandling handlade om strategier för att tillsätta alkalimetaller till CIGS-skiktet och hur de kopplar både till förändringar i skiktets sammansättning och solcellers verkningsgrader. Slutligen har jag analyserat hur en ytbehandling innehållande kaliumfluorid (KF) kan optimeras för CIGS-skikt, som innehåller små mängder silver (ACIGS). Jag kunde visa att en alltför omfattande behandling med KF var skadlig för verkningsgraden och korrelerade både med förekomst av sekundära faser i ACIGS-filmen, men framför allt med ett tjockare modifierat ytskikt än det som fanns i referenserna med god verkningsgrad.

I avhandlingsarbetet har användningen av elektronmikroskopi varit central för att analysera små lokala förändringar i de olika proverna. Sådana förändringar uppstår vanligen i nanometerskala och långt ner under provets yta, men de kan ha stor inverkan på solcellernas elektriska egenskaper. Analys av

provers kristallina egenskaper, kombinerade med kemisk sammansättning via de två huvudteknikerna EELS (electron energy loss spectroscopy), samt EDS (energy despersive X-ray spectroscopy) ledde till en förbättrad förståelse av solcellerna och till att vi fick revidera våra modeller. Eftersom elektronmikroskopitekniker vanligen innebär provpreparering, i mitt fall med FIB (fokuserande jonstråle), har stor vikt lagts på att undersöka och identifiera den procedur som ger den högsta kvalitén på proverna och den bästa reproducerbarheten. Ett viktigt resultat från detta arbete har varit att jag kunnat visa att det sista polersteget i provprepareringen kunde leda till en utbytesreaktion mellan Cu från CIGS-skiktet och Cd från buffertskiktet och hur detta problem kan undvikas. Ett sätt att öka förtroendet för att sammansättningsanalyserna har varit korrekta har varit att använda komplementära analystekniker som korsreferenser.

Elektronmikroskopi har redan bidragit med många viktiga pusselbitar för vår förståelse av solcellerna. Icke desto mindre finns det fortfarande många frågor kvar rörande till exempel halvledarnas interna elektriska fält och lokala bandstrukturer före och efter diverse olika behandlingar, som förtjänar ytterligare undersökningar.

*Framtidsperspektiv*

Energi är en fysikalisk storhet, som är inblandad i all omvandling. Alla våra grundläggande behov kräver utvinning, bearbetning, omvandling och transport av material. Därför är energi – både insamling och omvandling – så centralt. De fossila bränslena har, eller kommer inom kort att nå sin högsta möjliga utvinningsnivå och därefter kommer tillgången att minska. Det kommer leda till att vår och framtida generationer behöver anpassa sig till minskat tillgång till de mest lättillgängliga energislagen. Klimatpolitik kan också i ökad utsträckning bidra till att fossila bränsle görs dyrare än alternativen. Vidare verkar energipolitiken utvecklas och intresserar sig för nya energikällor.

Av detta följer att ett brett utbud av alternativa energislag utvecklas. Dessa är dock inte likvärdiga. För att kunna bedöma konkurrenskraften för olika alternativ och fatta kloka beslut behöver man använda olika typer av verktyg, såsom hur mycket energi man får tillbaka från varje investerad kWh (EROI) eller hur lång tid det tar innan en energiinvestering har betalat tillbaka sin energi (EPBT, eller energiåterbetalningstid). Andra viktiga aspekter är hur tillverkningen påverkar miljön och om det finns begränsningar i tillgång på de material som används i solcellerna. Idag diskuteras i stor utsträckning prissättning på olika energislag och hur de bidrar till utsläpp till atmosfären. Min slutsats är att det finns en god chans att koldioxidfria energislag, såsom kärnkraft, vattenkraft, vindkraft och solcellsbaserade system kommer att växa på bekostnad av den idag dominerande fossilbränslebaserade energin.

Genom att använda elektronmikroskopi, har jag försökt dra mitt strå till stacken genom att bidra till förståelsen och utvecklingen av tunnfilmssolceller och därmed plantera mitt blygsamma träd i den existerande kunskapsskogen.

# 8 Conclusion et perspectives en Français

Parmi les cellules solaires photovoltaïques (PV) à simple jonction, la branche des couches minces que j'ai étudiée avec cette thèse compte parmi les rendements de conversion les plus élevés (environ 23%), le plus grand taux de retour énergétique (EROI), un large choix de substrats possibles et un grand potentiel d'industrialisation. Bien que la maximisation du rendement des cellules solaires photovoltaïques soit une préoccupation majeure en laboratoire, elle n'est pas l'unique sujet de recherche. La réduction de l'épaisseur de l'absorbeur solaire ainsi que l'utilisation de substrats alternatifs tels que l'acier à la place du verre sodocalcique (SLG) ont été étudiés durant cette thèse. Pour ce faire, j'ai travaillé sur le développement de différentes couches intermédiaires et sur des traitements de surface, les deux ayant pour but, soit de passiver les interfaces, soit de bloquer des diffusions néfastes provenant du substrat en acier ; le tout ayant pour objectif de maintenir le rendement de conversion des cellules par rapport aux cellules solaires de référence.

Pour être plus concret, ce travail a mis en évidence l'effet positif d'une couche intermédiaire d'$Al_2O_3$ utilisé pour passiver l'interface entre l'absorbeur solaire et le contact arrière en Mo, mais aussi sa détérioration lorsque celle-ci est mise directement en contact avec un précurseur de NaF. En outre, j'ai analysé les défauts typiquement présents dans les couches barrières utilisées pour bloquer les diffusions néfastes lors de l'emploi de substrats en acier. J'ai montré que ces défauts pouvaient agir comme des chemins de diffusion et j'ai identifié qu'ils étaient initialement liés au processus de fabrication de l'acier. Un troisième volet de ma thèse concernait les différentes stratégies d'incorporation des métaux alcalins dans la couche absorbante CIGS, et leurs liens avec à la fois les changements de composition des couches et les rendements des cellules solaires. Pour terminer, j'ai analysé l'importance de l'intensité du post-traitement au KF appliqué à une couche d'absorbant CIGS alliée avec de l'argent (ACIGS). J'ai pu conclure qu'un traitement excessif était tout à fait préjudiciable pour le rendement de la cellule, et corrélait à la fois avec la présence de phases secondaires dans l'absorbeur solaire et avec une couche superficielle altérée plus épaisse.

Au cours de cette thèse, l'utilisation de la microscopie électronique était essentielle pour examiner les changements locaux au sein des différents échantillons. Ces modifications se produisent généralement à l'échelle du

nanomètre et le plus souvent en profondeur sous la surface de l'échantillon, mais elles peuvent fortement influencer le comportement électrique des cellules solaires. L'analyse de la cristallinité combinée à celle de la composition chimique via les techniques EELS et EDS ont permis d'améliorer notre compréhension des échantillons et de réviser nos modèles. Et parce que les techniques de microscopie électronique requièrent généralement une préparation des échantillons, des efforts importants ont été déployés pour identifier et contrôler les éventuels artefacts de préparation, ceci pour créer une préparation standard qualitative utilisant un FIB. Grâce à cela, j'ai pu montrer que le Cu de la couche CIGS pouvait diffuser artificiellement dans la couche de CdS pendant l'étape de polissage et en modifier la composition. Mais d'une manière générale, j'ai essayé de corréler les résultats de l'analyse microscopique avec d'autres techniques d'analyse pour améliorer le niveau de confiance de mes conclusions.

Les analyses en microscopie électronique ont déjà révélé de précieuses informations. Néanmoins, des questions concernant l'état du champ électrique interne des semi-conducteurs et la valeur de bande interdite locale avant et après les différents traitements demeurent et mériteraient des analyses plus poussées.

*Autres perspectives*

L'énergie est une quantité physique impliquée dans toute transformation. Tous nos besoins de base nécessitent l'extraction, la mise en forme, la transformation et le transport de matière, ce qui justifie l'importance majeure de la collection d'énergie et de sa conversion. En outre, certains des combustibles fossiles atteignent leur pic de production, ce qui signifie que notre génération et les futures doivent faire face à une restriction d'accès aux énergies les plus facilement accessibles. De plus, les politiques énergétiques semblent également évoluer et s'intéresser à dénicher de nouvelles sources d'énergie.

Par conséquent, un large panel de systèmes de conversion d'énergie alternatifs est en cours de développement. Mais ils ne sont pas tous équivalents. Pour juger de la viabilité des alternatives, j'inclurais deux valeurs scientifiques dans la boucle de décision: EROI et EPBT, qui quantifient la rentabilité énergétique d'une solution et la vitesse à laquelle l'énergie investie peut être retournée, respectivement. Cependant, les pollutions associées à chacune ainsi que leur disponibilité à long terme doivent également être prises en compte. De nos jours, les principales préoccupations sont le prix et les émanations atmosphériques. Il y a donc de fortes chances d'observer une croissance des systèmes nucléaires, hydroélectriques, éoliens et solaires au détriment des combustibles fossiles dominants.

En utilisant principalement la microscopie électronique, j'ai essayé de contribuer à la compréhension et au développement des cellules solaires en couches minces, ajoutant ainsi mon modeste arbre à la forêt de connaissance déjà existante.

# 9 Acknowledgements / Remerciements

A thesis is this lonely journey we went on together with many great people. There are several of the most important for me, and I already apologize for those I could have forgotten to name here: be sure you have a place in my heart anyway.

*Dear Supervisors*

**Lionel** It is always a pleasure to exchange with you, professionally like personally. You helped me growing up and despite the distance you were here when I needed it. Thanks for the advices, the guidance and the trust you provided during all these years. You are my spiritual big brother.

**Marika** Your sharp mind added to a will of feeding my ignorance was all I needed during this journey. There is no such a thing as "good or bad" supervisors, but I believe there are sometimes better matches than others. You are knowledgeable, responsive, extremely positive and human (and all at the same time!). Thank you for having accepted me among your working forces.

**Tom** I start to believe that your blood contains more electrons than actual blood cells, but I still wonder if it was a gift from birth or if you have built it over time. Your expertise has been essential for my progress and the guidance you provided me with was most precious. Thank you for answering all the questions I came up with and for the all the good discussions, even not related to work.

**Klaus** Thank you for offering me the opportunity to work in academia and introducing me to the world of electron microscopy. You offered me precious advices that I still keep with me.

*Dear Co-workers*

**Shi-Li, Zhen** Thank you for the reviews and comments that contributed to the quality of this work.

**Uwe Z** your execrable mood was not sufficient to retain me from repeatedly coming to you. Your deep knowledge of the tools and the network and the scripts and the electronic systems and the how stuff works and your particular will to *do* things, more than talking about them are definitely and strongly

contributing to maintaining the high standards of the group. (I wrote exactly as you said, but are you sure it will get you a salary rise?)

**Timo** Thanks for all your guidance concerning the electron microscopy and the sample preparation. It was bliss to share the small talks about life and more.

**Jörgen** Your door has always been open and I really appreciated it. Thanks for the help and the support during harsher times.

**Ingrid R. and Maria S.** From your office upstairs you always kept an eye on us. Thank you for all your support and explanations.

**Lars S.** It was always instructive to speak with you and I only regret that we could not do it more often. If I may offer you a piece of advice here, you are exceptionally good with solar cells but please call someone in the future if you consider again cutting down a tree.

**Lars R.** What a relief for me to see you accepting the TEM expert position! Thank you for the experience sharing and for unloading me from the analysis requests. It was a pleasure to teach you the FIB.

**Stefano** You were the first to hold my hand to the TEM room and to assist my first steps down there. Thank you for the interesting exchanges about everything and for the weekly D&D experience that no-one could lead as good as you did!

**Tobias B.** Our visit to the police station is still anchored in my mind. Thanks again for everything.

**Jan-Åke** The new students have no idea of how much they will miss without you. Your practical help was essential to most of the quality lab work I could have done.

**Delphine** That was an honor to be your cosplay photographer! Thanks for the exiting adventure.

**Sven E.** Thanks for all the exciting exchange we have had, you are officially a stress manager expert. And keep on baking amazing cakes!

**Tove** I am glad I could share this writing experience with you! Thanks for the good tips and chats.

**Victoria and Fredric E.** Thank you for the help you provided when I was stuck with a microscope.

**Fredrik** and **Tobias** It was a pleasure to talk and write with you. Thanks for the good time.

**Ray** Thank you for coming so often asking me random questions about everything. For the rest, I will keep in mind this one night we spent together, and it's not only a legend, you snore.

**Jan** Your dedication to work was impressive and you often had good advices to share. One day you might rule the place.

**Uwe S** Your presence in the lab was important both for keeping the grandma'BAK running and for keeping the good mood up. Thanks for all the chats we have had.

**Petra, Ling, Patrick, Syaiful, Björn** You have been great neighbors during these years of study and I was glad to sit close to you. Thanks for being so nice, for the time shared and the good discussions.

**Tomas** I want to acknowledge your help with the student supervision, thanks for the management advices.

**Alexandra** Your constant smile, even when sadness seemed to take over, lightened several of my working days. Thank you for this.

Thanks to all the Solcellers and colleagues that I was happy to meet and glad to know, **Carl, Céline, Sara, Ramy, Jonathan, Pedro, Charlotte, Adam, Dragos, Hu, Hassan, Nina, Michael, Kaspar, Katarina, Lukas, Faraz, Pia, Jes, Olof, Nishant, Malkolm, Wei-Chao, Dorothea, Mauricio, Aqib, Ishtiaq**…

**The random guy** at my daughter's friend birthday party: your practical questions about the type of inverters you would need for your PV installation helped me realizing how little I knew once I stepped aside from my field, even for what appeared to be a small step.

*Dear Friends (those who have chosen to be around)*

**Marion et Florent**, **Mathieu et Claire**, **Aeneas**, **Nicolas et Anaïs**, **Annaick et Ludovic, Kate and Oleg, Patrice et Pauline, Liane and Sven, Elsa et Lionel**. Thank you, merci pour votre soutien, pour les nombreux échanges que l'on a eu et les discussions passionnées (sur le jardinage même au cœur

de l'hiver Suédois!), merci également pour les nombreux jeux de plateau. Merci d'être aussi ouverts et de m'apporter autant.

*Dear Family (those who haven't chosen much)*
My parents, **Cécile et François,** and my brother, **Thomas.** You didn't always understand what I was doing but you were not far away looking after me. Merci d'avoir accepté mon depart à l'étranger, de supporter mes critiques scientifiques, merci d'être venu me rendre visite jusqu'ici et merci d'être toujours là pour moi.

My parents in law, **Catherine et Bertrand**. Who wouldn't dream of having parents in law like you? Merci d'avoir été presents durant ces années, merci pour tous nos échanges, votre ouverture et votre soutien.

My kids, **Emmanuelle et Gabriel** thank you for being kids and for having brought me down back to life when it was needed. Merci d'avoir rythmé mes jours et mes nuits afin de me tenir les pieds sur terre et le sourire aux lèvres.

My dear wife, **Lucie** How could I thank correctly the person who accepted to share with me the joy and the burden of life? You offered me love, support, care, advices, guidance and you even stored food for me in the freezer so I wouldn't dry out during this thesis writing! Merci pour les discussions passionnantes [1], pour ton soutien logistique et moral. Merci pour tout ce que tu m'apportes <3.

[1] Dans au moins 56% des cas (*source: lesstatistiquesaupif.com*)

# 10 References


1. IEA. *Electricity Information Statistics*.; 2018. doi:10.1787/elect-data-en.
2. Enerdata. Global Energy Statistical Yearbook. *2018*. Available at: https://yearbook.enerdata.net/renewables/wind-solar-share-electricity-production.html. Accessed August 1, 2018.
3. British Petroleum. BP Statistical Review of World Energy 2017. *Br. Pet.* 2017;(66):1-52.
4. Department of Infrastructure T, Government RD and L, Canberra A. *Transport Energy Futures: Long-Term Oil Supply Trends and Projections Report 117*. Canberra: Bureau of Infrastructure, Transport and Regional Economics (BITRE); 2009.
5. Bhandari KP, Collier JM, Ellingson RJ, Apul DS. Energy payback time (EPBT) and energy return on energy invested (EROI) of solar photovoltaic systems: A systematic review and meta-analysis. *Renew. Sustain. Energy Rev.* 2015;47:133-141. doi:10.1016/j.rser.2015.02.057.
6. Peter LM. Towards sustainable photovoltaics: the search for new materials. *Philos. Trans. R. Soc. A Math. Phys. Eng. Sci.* 2011;369(1942):1840-1856. doi:10.1098/rsta.2010.0348.
7. Lindahl J. *National Survey Report of PV Power Applications in SWEDEN 2016*.; 2016. doi:10.13140/RG.2.2.23848.26887.
8. Martin A. Green, Keith Emery, Yoshihiro Hishikawa, Wilhelm Warta EDD. Solar cell efficiency tables. *Prog. Photovolt Res. Appl.* 2016;24:905-913.
9. Pern FJ, Noufi R. Stability of CIGS solar cells and component materials evaluated by a step-stress accelerated degradation test method. 2012;8472(October):84720J-84720J-14. doi:10.1117/12.930541.
10. Kurtz S, Repins I, Metzger WK, et al. Historical Analysis of Champion Photovoltaic Module Efficiencies. *IEEE J. Photovoltaics* 2018;8(2):363-372. doi:10.1109/JPHOTOV.2018.2794387.
11. Reinhard P, Chirila A, Blosch P, et al. Review of Progress Toward 20% Efficiency Flexible CIGS Solar Cells and Manufacturing Issues of Solar Modules. *IEEE J. Photovoltaics* 2013;3(1):572-580. doi:10.1109/JPHOTOV.2012.2226869.
12. Sze SM, Ng KK. *Physics of Semiconductor Devices - Third Edition*. Wiley; 2006.
13. Würfel P. *Physics of Solar Cells*. (Wrfel P, ed.). Weinheim, Germany: Wiley-VCH Verlag GmbH; 2005. doi:10.1002/9783527618545.
14. Pierret RF. *Semiconductor Device Fundamentals*. Addison-Wesley; 1996.
15. Falkowski PG. The Evolution of Modern Eukaryotic Phytoplankton. *Science (80-. ).* 2004;305(5682):354-360. doi:10.1126/science.1095964.
16. Abou-Ras D, Wagner S, Stanbery BJ, et al. Innovation highway: Breakthrough milestones and key developments in chalcopyrite photovoltaics from a retrospective viewpoint. *Thin Solid Films* 2017:1-11. doi:10.1016/j.tsf.2017.01.005.

17. Lindahl J, Keller J, Donzel-Gargand O, Szaniawski P, Edoff M, Törndahl T. Deposition temperature induced conduction band changes in zinc tin oxide buffer layers for Cu(In,Ga)Se2solar cells. *Sol. Energy Mater. Sol. Cells* 2016;144:684-690. doi:10.1016/j.solmat.2015.09.048.
18. Burgelman M, Nollet P, Degrave S. Modelling polycrystalline semiconductor solar cells. *Thin Solid Films* 2000;361-362:527-532. doi:10.1016/S0040-6090(99)00825-1.
19. King RR, Hong W, Fetzer CM, et al. Fundamental Efficiency Losses in Next-Generation Multijunction Solar Cells. *25th Eur. Photovolt. Sol. Energy Conf. Proceeding* 2010:1-4.
20. Polman A, Knight M, Garnett EC, Ehrler B, Sinke WC. Photovoltaic materials: Present efficiencies and future challenges. *Science (80-. ).* 2016;352(6283):aad4424-aad4424. doi:10.1126/science.aad4424.
21. ASTM International. *ASTM G173-03(2012), Standard Tables for Reference Solar Spectral Irradiances: Direct Normal and Hemispherical on 37° Tilted Surface*. West Conshohocken, PA; 2012. doi:10.1520/G0173-03R12.
22. Herberholz R, Nadenau V, Rühle U, Köble C, Schock HW, Dimmler B. Prospects of wide-gap chalcopyrites for thin film photovoltaic modules. *Sol. Energy Mater. Sol. Cells* 1997;49(1-4):227-237. doi:10.1016/S0927-0248(97)00199-2.
23. Khatri I, Shudo K, Matsuura J, Sugiyama M, Nakada T. Impact of heat-light soaking on potassium fluoride treated CIGS solar cells with CdS buffer layer. *Prog. Photovoltaics Res. Appl.* 2018;26(3):171-178. doi:10.1002/pip.2962.
24. Jackson P, Hariskos D, Wuerz R, Wischmann W, Powalla M. Compositional investigation of potassium doped Cu(In,Ga)Se2 solar cells with efficiencies up to 20.8%. *Phys. Status Solidi - Rapid Res. Lett.* 2014;8(3):219-222. doi:10.1002/pssr.201409040.
25. Edoff M, Jarmar T, Nilsson NS, et al. High $V_{oc}$ in (Cu,Ag)(In,Ga)$Se_2$ Solar Cells. *IEEE J. Photovoltaics* 2017;7(6):1789-1794. doi:10.1109/JPHOTOV.2017.2756058.
26. Zhang R, Hollars D, Kanicki J. High Efficiency Cu (In, Ga) Se2 Flexible Solar Cells Fabricated by Roll-to-Roll Metallic Precursor Co-sputtering Method. *Jap. J. Appl. Phys.* 2013;52:1-10. Available at: UNSP 092302.
27. Green MA, Hishikawa Y, Dunlop ED, Levi DH, Hohl-Ebinger J, Ho-Baillie AWY. Solar cell efficiency tables (version 52). *Prog. Photovoltaics Res. Appl.* 2018;26(7):427-436. doi:10.1002/pip.3040.
28. Wuerz R, Eicke a., Frankenfeld M, et al. CIGS thin-film solar cells on steel substrates. *Thin Solid Films* 2009;517(7):2415-2418. doi:10.1016/j.tsf.2008.11.016.
29. Eisenbarth T, Caballero R, Kaufmann CA, Eicke A, Unold T. Influence of iron on defect concentrations and device performance for Cu(In,Ga)Se2 solar cells on stainless steel substrates. *Prog. Photovoltaics Res. Appl.* 2012;20(5):568-574. doi:10.1002/pip.2260.
30. Wuerz R, Eicke a., Kessler F, Pianezzi F. Influence of iron on the performance of CIGS thin-film solar cells. *Sol. Energy Mater. Sol. Cells* 2014;130:107-117. doi:10.1016/j.solmat.2014.06.038.
31. Blösch P, Pianezzi F, Chirilă a., et al. Diffusion barrier properties of molybdenum back contacts for Cu(In,Ga)Se2 solar cells on stainless steel foils. *J. Appl. Phys.* 2013;113(5):054506. doi:10.1063/1.4789616.
32. Wuerz R, Eicke a., Kessler F, Rogin P, Yazdani-Assl O. Alternative sodium sources for Cu(In,Ga)Se2 thin-film solar cells on flexible substrates. *Thin Solid Films* 2011;519(21):7268-7271. doi:10.1016/j.tsf.2011.01.399.

33. Herz K, Eicke a., Kessler F, Wächter R, Powalla M. Diffusion barriers for CIGS solar cells on metallic substrates. *Thin Solid Films* 2003;431-432:392-397. doi:10.1016/S0040-6090(03)00259-1.
34. Herz K, Kessler F, Wächter R, Powalla M. Dielectric barriers for flexible CIGS solar modules. *Thin Solid Films* 2002;404:384-389.
35. Wuerz R, Eicke a., Kessler F, Paetel S, Efimenko S, Schlegel C. CIGS thin-film solar cells and modules on enamelled steel substrates. *Sol. Energy Mater. Sol. Cells* 2012;100:132-137. doi:10.1016/j.solmat.2012.01.004.
36. Platzer-Björkman C, Jani S, Westlinder J, Linnarsson MK, Scragg J, Edoff M. Diffusion of Fe and Na in co-evaporated Cu(In,Ga)Se2 devices on steel substrates. *Thin Solid Films* 2013;535(1):188-192. doi:10.1016/j.tsf.2012.11.067.
37. F. Pianezzi*, A. Chirilă, P. Blösch, S. Seyrling, S. Buecheler, L. Kranz CF and ANT. Electronic properties of Cu (In, Ga) Se2 solar cells on stainless steel foils without diffusion barrier. *Prog. Photovoltaics Res. Appl.* 2012;20(January):253-259. doi:10.1002/pip.1247.
38. Zunger A, Zhang SB, Wei S-H. Why is CuInSe2 tolerant to defects and what is the origin of "Ordered Defect Structures." In: *AIP Conference Proceedings*.Vol 394. AIP; 1997:63-74. doi:10.1063/1.52886.
39. Lany S, Zunger A. Intrinsic DX centers in ternary chalcopyrite semiconductors. *Phys. Rev. Lett.* 2008;100(1):1-4. doi:10.1103/PhysRevLett.100.016401.
40. Lany S, Zunger A. Light- and bias-induced metastabilities in Cu(In,Ga)Se2based solar cells caused by the (VSe-VCu) vacancy complex. *J. Appl. Phys.* 2006;100(11). doi:10.1063/1.2388256.
41. Erslev P, Hanket GM, Shafarman WN, Cohen DJ. Characterizing the effects of silver alloying in chalcopyrite CIGS with junction capacitance methods. *MRS Proc.* 2009;1165:1165-M01-07. doi:10.1557/PROC-1165-M01-07.
42. Boyle J, Hanket G, Shafarman W. Optical and quantum efficiency analysis of (Ag,Cu)(In,Ga)$Se_2$ absorber layers. In: *2009 34th IEEE Photovoltaic Specialists Conference (PVSC)*. IEEE; 2009:001349-001354. doi:10.1109/PVSC.2009.5411272.
43. Kim K, Ahn SK, Choi JH, et al. Highly efficient Ag-alloyed Cu(In,Ga)Se2solar cells with wide bandgaps and their application to chalcopyrite-based tandem solar cells. *Nano Energy* 2018;48(March):345-352. doi:10.1016/j.nanoen.2018.03.052.
44. Chen S, Gong X, Wei S-H. Band-structure anomalies of the chalcopyrite semiconductors CuGaX2 versus AgGaX2 (X=S and Se) and their alloys. *Phys. Rev. B* 2007;75(20):205209. doi:10.1103/PhysRevB.75.205209.
45. Boyle JH, McCandless BE, Shafarman WN, Birkmire RW. Structural and optical properties of (Ag,Cu)(In,Ga)Se2 polycrystalline thin film alloys. *J. Appl. Phys.* 2014;115(22). doi:10.1063/1.4880243.
46. Shafarman W, Thompson C, Boyle J, Hanket G, Erslev P, Cohen JD. Device characterization of (AgCu)(InGa) Se2 solar cells. In: *Photovoltaic Specialists Conference (PVSC), 2010 35th IEEE*. IEEE; 2010:000325–000329.
47. Hanket G, Boyle JH, Shafarman WN. Characterization and device performance of (AgCu)(InGa)Se2 absorber layers. *2009 34th IEEE Photovolt. Spec. Conf.* 2009:001240-001245.
48. Salomé PMP, Rodriguez-alvarez H, Sadewasser S. Cells Incorporation of alkali metals in chalcogenide solar cells. *Sol. Energy Mater. Sol. Cells* 2015;143:9-20. doi:10.1016/j.solmat.2015.06.011.

49. Forest R V., Eser E, McCandless BE, Chen JG, Birkmire RW. Reversibility of (Ag,Cu)(In,Ga)Se2 electrical properties with the addition and removal of Na: Role of grain boundaries. *J. Appl. Phys.* 2015;117(11). doi:10.1063/1.4915334.
50. Wei S, Zhang SB, Zunger A, Wei S, Zhang SB, Zunger A. Effects of Na on the electrical and structural properties of Effects of Na on the electrical and structural properties of CuInSe 2. 1999;7214. doi:10.1063/1.370534.
51. Aguiar JA, Stokes A, Jiang C, et al. Revealing Surface Modifications of Potassium-Fluoride-Treated Cu(In,Ga)Se 2 : A Study of Material Structure, Chemistry, and Photovoltaic Performance. *Adv. Mater. Interfaces* 2016;3(17):1600013. doi:10.1002/admi.201600013.
52. Nicoara N, Lepetit T, Arzel L, Harel S, Barreau N, Sadewasser S. Effect of the KF post-deposition treatment on grain boundary properties in Cu(In, Ga)Se2 thin films. *Sci. Rep.* 2017;7(December 2016):41361. doi:10.1038/srep41361.
53. Yin W, Wu Y, Noufi R, Al-Jassim M, Yan Y. Defect segregation at grain boundary and its impact on photovoltaic performance of CuInSe 2. *Appl. Phys. Lett.* 2013;102(19):193905. doi:10.1063/1.4804606.
54. Braunger D, Hariskos D, Bilger G, Rau U, Schock HW. Influence of sodium on the growth of polycrystalline Cu(In, Ga)Se2 thin films. *Thin Solid Films* 2000;361-362:161-166. doi:http://dx.doi.org/10.1016/S0040-6090(99)00777-4.
55. Alonso MI, Garriga M, Durante Rincón CA, Hernández E, León M. Optical functions of chalcopyrite CuGa x In 1-x Se 2 alloys. *Appl. Phys. A Mater. Sci. Process.* 2002;74(5):659-664. doi:10.1007/s003390100931.
56. Gloeckler M, Sites JR. Potential of submicrometer thickness Cu(In,Ga)Se2 solar cells. *J. Appl. Phys.* 2005;98(10):103703. doi:10.1063/1.2128054.
57. Pistor P, Greiner D, Kaufmann CA, et al. Experimental indication for band gap widening of chalcopyrite solar cell absorbers after potassium fluoride treatment. *Appl. Phys. Lett.* 2014;105(6). doi:10.1063/1.4892882.
58. Handick E, Reinhard P, Alsmeier JH, et al. Potassium Postdeposition Treatment-Induced Band Gap Widening at Cu(In,Ga)Se2Surfaces - Reason for Performance Leap? *ACS Appl. Mater. Interfaces* 2015;7(49):27414-27420. doi:10.1021/acsami.5b09231.
59. Kotipalli R, Vermang B, Joel J, Rajkumar R, Edoff M, Flandre D. Investigating the electronic properties of $Al_2O_3$/Cu(In,Ga)$Se_2$ interface. *AIP Adv.* 2015;5:107101. doi:10.1063/1.4932512.
60. Williams DB, Carter CB. The Transmission Electron Microscope. In: *Transmision Electron Miscroscopy*. Boston, MA: Springer US; 2009:3-22. doi:10.1007/978-0-387-76501-3_1.
61. Dahmen U, Erni R, Kisielowki C, et al. An update on the TEAM project — first results from the TEAM 0.5 microscope, and its future development. In: *EMC 2008 14th European Microscopy Congress 1–5 September 2008, Aachen, Germany*. Berlin, Heidelberg: Springer Berlin Heidelberg; :3-4. doi:10.1007/978-3-540-85156-1_2.
62. Egerton RF. *Electron Energy-Loss Spectroscopy in the Electron Microscope*. Boston, MA: Springer US; 2011. doi:10.1007/978-1-4419-9583-4.
63. Reimer L, Kohl H. *Transmission Electron Microscopy Physics of Image Formation*.; 2008. doi:10.1007/978-0-387-34758-5.
64. Williams DB, Carter CB. *Transmission Electron Microscopy: A Textbook for Materials Science*.; 2009. doi:10.1007/978-1-61779-415-5_23.
65. Zou X, Hovmöller S, Oleynikov P. *Electron CrystallographyElectron Microscopy and Electron Diffraction*. Oxford University Press; 2011. doi:10.1093/acprof:oso/9780199580200.001.0001.

66. Klinger M, Jäger A. Crystallographic Tool Box ( CrysTBox ): automated tools for transmission electron microscopists and crystallographers. *J. Appl. Crystallogr.* 2015;48(6):2012-2018. doi:10.1107/S1600576715017252.
67. Ayache J, Beaunier L, Boumendil J, Ehret G, Laub D. *Sample Preparation Handbook for Transmission Electron Microscopy*. New York, NY: Springer New York; 2010. doi:10.1007/978-0-387-98182-6.
68. Rubino S, Akhtar S, Melin P, Searle A, Spellward P, Leifer K. A site-specific focused-ion-beam lift-out method for cryo Transmission Electron Microscopy. *J. Struct. Biol.* 2012;180(3):572-6. doi:10.1016/j.jsb.2012.08.012.
69. Langford RM, Rogers M. In situ lift-out: Steps to improve yield and a comparison with other FIB TEM sample preparation techniques. *Micron* 2008;39(8):1325-1330. doi:10.1016/j.micron.2008.02.006.
70. Langford RM, Clinton C. In situ lift-out using a FIB-SEM system. *Micron* 2004;35(7):607-611. doi:10.1016/j.micron.2004.03.002.
71. Schaffer M, Schaffer B, Ramasse Q. Sample preparation for atomic-resolution STEM at low voltages by FIB. *Ultramicroscopy* 2012;114:62-71. doi:10.1016/j.ultramic.2012.01.005.
72. Abou-Ras D, Marsen B, Rissom T, et al. Enhancements in specimen preparation of Cu(In,Ga)(S,Se)2 thin films. *Micron* 2012;43(2-3):470-474. doi:10.1016/j.micron.2011.11.004.
73. Ward BW, Notte JA, Economou NP. Helium ion microscope: A new tool for nanoscale microscopy and metrology. *J. Vac. Sci. Technol. B Microelectron. Nanom. Struct.* 2006;24(6):2871. doi:10.1116/1.2357967.
74. McCaffrey JP, Phaneuf MW, Madsen LD. Surface damage formation during ion-beam thinning of samples for transmission electron microscopy. *Ultramicroscopy* 2001;87(3):97-104. doi:10.1016/S0304-3991(00)00096-6.
75. Huh Y, Hong KJ, Shin KS. Amorphization Induced by Focused Ion Beam Milling in Metallic and Electronic Materials. *Microsc. Microanal.* 2013;19(S5):33-37. doi:10.1017/S1431927613012282.
76. Barna Á, Pécz B, Menyhard M. TEM sample preparation by ion milling/amorphization. *Micron* 1999;30(3):267-276. doi:10.1016/S0968-4328(99)00011-6.
77. Giannuzzi LA, Geurts R, Ringnalda J. 2 keV Ga+ FIB Milling for Reducing Amorphous Damage in Silicon. *Microsc. Microanal.* 2005;11(S02):2004-2005. doi:10.1017/S1431927605507797.
78. Ziegler JF, Ziegler MD, Biersack JP. SRIM – The stopping and range of ions in matter (2010). *Nucl. Instruments Methods Phys. Res. Sect. B Beam Interact. with Mater. Atoms* 2010;268(11-12):1818-1823. doi:10.1016/j.nimb.2010.02.091.
79. Park CM, Bain JA, Clinton TW, Van Der Heijden PAA, Klemmer TJ. Measurement of Ga implantation profiles in the sidewall and bottom of focused-ion-beam-etched structures. *Appl. Phys. Lett.* 2004;84(17):3331-3333. doi:10.1063/1.1715142.
80. Rao DVS, Muraleedharan K, Humphreys CJ. TEM specimen preparation techniques. *Education* 2010;(320):1232-1244.
81. Ishitani T, Kaga H. Calculation of Local Temperature Rise in Focused-Ion-Beam Sample Preparation. *J. Electron Microsc. (Tokyo).* 1995;44(5):331. doi:10.1093/oxfordjournals.jmicro.a051185.
82. Shukla N, Tripathi SK, Banerjee A, Ramana ASV, Rajput NS, Kulkarni VN. Study of temperature rise during focused Ga ion beam irradiation using nanothermo-probe. *Appl. Surf. Sci.* 2009;256(2):475-479. doi:10.1016/j.apsusc.2009.07.024.

83. Peach DF, Lane DW, Sellwood MJ. An assessment of surface heating during ion beam analysis I. Experimental method. *Nucl. Instruments Methods Phys. Res. Sect. B Beam Interact. with Mater. Atoms* 2006;249(1-2 SPEC. ISS.):677-679. doi:10.1016/j.nimb.2006.03.078.
84. Timo Wätjen J, Scragg JJ, Edoff M, Rubino S, Platzer-Björkman C. Cu out-diffusion in kesterites - A transmission electron microscopy specimen preparation artifact. *Appl. Phys. Lett.* 2013;102(5). doi:10.1063/1.4790282.
85. Drouin D, Couture AR, Joly D, Tastet X, Aimez V, Gauvin R. CASINO V2.42—A Fast and Easy-to-use Modeling Tool for Scanning Electron Microscopy and Microanalysis Users. *Scanning* 2007;29(3):92-101. doi:10.1002/sca.20000.
86. Altmann F, Schischka J, Lehmann R. Combined electron beam induced current imaging ( EBIC ) and focused ion beam ( FIB ) techniques for thin film solar cell characterization. *36th Int. Symp. Test. Fail. Anal.* 2010.
87. Zhang Z, Wagner T. Interfacial microstructure and defect analysis in Cu(In,Ga)Se([sub]2)-based multilayered film by analytical transmission electron microscopy and focused ion beam. *Thin Solid Films* 2009;517(15):4329-4335. doi:10.1016/j.tsf.2009.02.130.
88. Abou-Ras D, Kostorz G, Romeo A, Rudmann D, Tiwari AN. Structural and chemical investigations of CBD- and PVD-CdS buffer layers and interfaces in Cu(In,Ga)Se2-based thin film solar cells. *Thin Solid Films* 2005;480-481:118-123. doi:10.1016/j.tsf.2004.11.033.
89. He X, Varley J, Ercius P, et al. Intermixing and Formation of Cu-Rich Secondary Phases at Sputtered CdS/CuInGaSe2 Heterojunctions. *IEEE J. Photovoltaics* 2016;6(5):1308-1315. doi:10.1109/JPHOTOV.2016.2589362.
90. Salome PMP, Ribeiro-andrade R, Teixeira JP, et al. Cd and Cu Interdiffusion in Cu ( In , Ga ) Se 2 / CdS. *IEEE J. Photovoltaics* 2017;7(3):1-6.
91. Ishizuka S, Sakurai K, Yamada A, et al. Fabrication of wide-gap Cu(ln(1-x)Ga(x))Se2 thin film solar cells: a study on the correlation of cell performance with highly resistive i-ZnO layer thickness. *Sol. Energy Mater. Sol. Cells* 2005;87:541-548. doi:10.1016/j.solmat.2004.08.017.
92. Rau U, Schmidt M. Electronic properties of ZnO/CdS/Cu(In,Ga)Se2 solar cells - Aspects of heterojunction formation. *Thin Solid Films* 2001;387(1-2):141-146. doi:10.1016/S0040-6090(00)01737-5.
93. Scheer R, Messmann-Vera L, Klenk R, Schock HW. On the role of non-doped ZnO in CIGSe solar cells. *Prog. Photovoltaics Res. Appl.* 2012;20(6):619-624. doi:10.1002/pip.1185.
94. Batchelor WK, Repins IL, Schaefer J, Beck ME. Impact of substrate roughness on CuInxGa1-xSe 2 device properties. *Sol. Energy Mater. Sol. Cells* 2004;83:67-80. doi:10.1016/j.solmat.2003.10.005.
95. Schulz A, Herrmann D, Kessler F, Schneider J, Walker M, Schumacher U. Detection and identification of pinholes in plasma-polymerised thin film barrier coatings on metal foils. *Surf. Coatings Technol.* 2005;200(1-4):213-217. doi:10.1016/j.surfcoat.2005.02.125.
96. Kessler F, Herrmann D, Powalla M. Approaches to flexible CIGS thin-film solar cells. *Thin Solid Films* 2005;480-481:491-498. doi:10.1016/j.tsf. 2004.11.063.
97. Shafarman WN, Stolt L. *Cu ( InGa ) Se 2 Solar Cells*.; 2003.

Acta Universitatis Upsaliensis

*Digital Comprehensive Summaries of Uppsala Dissertations from the Faculty of Science and Technology* 1701

Editor: The Dean of the Faculty of Science and Technology

A doctoral dissertation from the Faculty of Science and Technology, Uppsala University, is usually a summary of a number of papers. A few copies of the complete dissertation are kept at major Swedish research libraries, while the summary alone is distributed internationally through the series Digital Comprehensive Summaries of Uppsala Dissertations from the Faculty of Science and Technology. (Prior to January, 2005, the series was published under the title "Comprehensive Summaries of Uppsala Dissertations from the Faculty of Science and Technology".)

Distribution: publications.uu.se
urn:nbn:se:uu:diva-357127

ACTA
UNIVERSITATIS
UPSALIENSIS
UPPSALA
2018